Received: 6 February 2024 | Revised: 17 June 2024 | Accepted: 10 July 2024

DOI: 10.1002/cac2.12595

ORIGINAL ARTICLE

CANCER COMMUNICATIONS Open Access

Targeting N4-acetylcytidine suppresses hepatocellular carcinoma progression by repressing eEF2-mediated HMGB2 mRNA translation

Hailing Liu[1,2] | **Lei Xu**[1,2] | **Shiwei Yue**[1,2] | **Hongfei Su**[1,2] | **Xing Chen**[3] | **Qiumeng Liu**[1,2] | **Hui Li**[4] | **Huifang Liang**[1,2] | **Xiaoping Chen**[1,2,5] | **Jiefeng He**[6] | **Zeyang Ding**[1,2] | **Bixiang Zhang**[1,2,5]

[1]Hepatic Surgery Center, Tongji Hospital, Tongji Medical College, Huazhong University of Science and Technology, Wuhan, Hubei, P. R. China

[2]Hubei Key Laboratory of Hepato-Pancreatic-Biliary Diseases, Tongji Hospital, Tongji Medical College, Huazhong University of Science and Technology, Wuhan, Hubei, P. R. China

[3]Department of Hepatopancreatobiliary Surgery, Zhejiang Cancer Hospital, Hangzhou Institute of Medicine (HIM), Chinese Academy of Sciences, Hangzhou, Zhejiang, P. R. China

[4]Department of Hepatobiliary Pancreatic Tumor Center, Chongqing University Cancer Hospital, School of Medicine, Chongqing University, Chongqing, P. R. China

[5]Key Laboratory of Organ Transplantation, Ministry of Education, Wuhan, Hubei, P. R. China

[6]Department of Hepatobiliary Surgery, Key Laboratory of Hepatobiliary and Pancreatic Diseases of Shanxi Province (Preparatory), Shanxi Bethune Hospital, Shanxi Academy of Medical Sciences, Shanxi Medical University, Taiyuan, Shanxi, P. R. China

Correspondence
Bixiang Zhang, Hepatic Surgery Center, Tongji Hospital, Tongji Medical College, Huazhong University of Science and Technology, Wuhan, Hubei, P. R. China.
Email: bixiangzhang@hust.edu.cn

Zeyang Ding, Hepatic Surgery Center, Tongji Hospital, Tongji Medical College, Huazhong University of Science and Technology, Wuhan, Hubei, P. R. China.
Email: zyding@tjh.tjmu.edu.cn

Abstract

Background: N4-acetylcytidine (ac4C) represents a novel messenger RNA (mRNA) modification, and its associated acetyltransferase N-acetyltransferase 10 (NAT10) plays a crucial role in the initiation and progression of tumors by regulating mRNA functionality. However, its role in hepatocellular carcinoma (HCC) development and prognosis is largely unknown. This study aimed to elucidate the role of NAT10-mediated ac4C in HCC progression and provide a promising therapeutic approach.

Abbreviations: ac4C, N4-acetylcytidine; acRIP-seq, acetylated RNA immunoprecipitation and sequencing; CCK-8, Cell Counting Kit-8; CDS, coding sequence; CETSA, cellular thermal shift assay; CPTAC, The Clinical Proteomic Tumor Analysis Consortium; DARTS, drug affinity responsive targets stability assay; DIA, data-independent acquisitio proteomics quantification; eEF2, eukaryotic Elongation Factor 2; EV71, enterovirus 71; GO, Gene ontology analysis; HCC, hepatocellular carcinoma; HMGB2, High Mobility Group Protein B2; IC50, a half-maximal inhibitory concentration; IHC, Immunohistochemistry; MCS, multiple cloning site; mRNA, messenger RNA; NAT10, N-acetyltransferase 10; OS, overall survival; PPI, protein–protein interaction; qPCR, quantitative PCR; RFS, recurrence-free survival; Ribo-seq, ribosome profiling analyses; RIP, RNA immunoprecipitates; RNA-seq, RNA sequencing; RPF, ribosome protected fragment; siRNA, small interfering RNA; SPR, surface plasmon resonance; SUnSET, Surface sensing of translation assay; T.E, translation efficiency; TCGA, The Cancer Genome Atlas Program; TIME, tumor immune microenvironment; TUNEL, terminal deoxynucleotidyl transferase–mediated deoxyuridine triphosphate nick-end labeling; UTR, untranslated regions; VEGF, vascular endothelial growth factor.

Jiefeng He, Department of Hepatobiliary Surgery, Key Laboratory of Hepatobiliary and Pancreatic Diseases of Shanxi Province (Preparatory), Shanxi Bethune Hospital, Shanxi Academy of Medical Sciences, Shanxi Medical University, Taiyuan, Shanxi, P. R. China.
Email: hejiefeng2008@163.com

Xiaoping Chen, Hepatic Surgery Center, Tongji Hospital, Tongji Medical College, Huazhong University of Science and Technology, Wuhan, Hubei, P. R. China.
Email: chenxp@tjh.tjmu.edu.cn

Funding information
State Key Project on Infection Disease of China, Grant/Award Number: 2018ZX10723204-003-003; Tongji Hospital (HUST) Foundation for Excellent Young Scientist, Grant/Award Number: 2020YQ05; National Basic Research Program of China, Grant/Award Number: 2020YFA0710700; Knowledge Innovation Program of Wuhan-Shuguang Project, Grant/Award Number: 2022020801020456; the first level of the public health youth top talent project of Hubei province, Grant/Award Number: 2022SCZ051; National Natural Science Foundation of China, Grant/Award Numbers: 81874065, 81874189, 82203823, 82273441

Methods: The ac4C levels were evaluated by dot blot and ultra-performance liquid chromatography-tandem mass spectrometry with harvested HCC tissues. The expression of NAT10 was investigated using quantitative real-time polymerase chain reaction, western blotting, and immunohistochemical staining across 91 cohorts of HCC patients. To explore the underlying mechanisms of NAT10-ac4C in HCC, we employed a comprehensive approach integrating acetylated RNA immunoprecipitation and sequencing, RNA sequencing and ribosome profiling analyses, along with RNA immunoprecipitation, RNA pull-down, mass spectrometry, and site-specific mutation analyses. The drug affinity responsive targets stability, cellular thermal shift assay, and surface plasmon resonance assays were performed to assess the specific binding of NAT10 and Panobinostat. Furthermore, the efficacy of targeting NAT10-ac4C for HCC treatment was elucidated through in vitro experiments using HCC cells and in vivo HCC mouse models.

Results: Our investigation revealed a significant increase in both the ac4C RNA level and NAT10 expression in HCC. Notably, elevated NAT10 expression was associated with poor outcomes in HCC patients. Functionally, silencing NAT10 suppressed HCC proliferation and metastasis in *vitro* and in vivo. Mechanistically, NAT10 stimulates the ac4C modification within the coding sequence (CDS) of high mobility group protein B2 (HMGB2), which subsequently enhances HMGB2 translation by facilitating eukaryotic elongation factor 2 (eEF2) binding to the ac4C sites on HMGB2 mRNA's CDS. Additionally, high-throughput compound library screening revealed Panobinostat as a potent inhibitor of NAT10-mediated ac4C modification. This inhibition significantly attenuated HCC growth and metastasis in both in vitro experiments using HCC cells and in vivo HCC mouse models.

Conclusions: Our study identified a novel oncogenic epi-transcriptome axis involving NAT10-ac4C/eEF2-HMGB2, which plays a pivotal role in regulating HCC growth and metastasis. The drug Panobinostat validates the therapeutic potential of targeting this axis for HCC treatment.

KEYWORDS
N4-acetylcytidine, N-acetyltransferase 10, hepatocellular carcinoma, mRNA translation, targeted therapy

1 | BACKGROUND

Hepatocellular carcinoma (HCC) ranks as the fourth leading cause of cancer-related mortality worldwide, presenting a high fatality rate [1]. Despite recent advancements in medical therapy for advanced HCC, the median survival rate remains below two years, even with the most effective treatments available [2–5]. This underscores a significant unmet need in medicine. Current therapeutic approaches for advanced HCC, such as atezolizumab (a programmed death-ligand 1 [PD-L1] inhibitor) combined with bevacizumab (an angiogenic inhibitor targeting vascular endothelial growth factor, VEGF), primarily target the tumor immune microenvironment (TIME) rather than directly addressing tumor cells [6, 7]. Therefore, there is an urgent need to identify novel biomarkers and therapeutic targets for HCC diagnosis and treatment.

The N4-acetylcytidine (ac4C) modification, initially observed predominantly in transfer RNA (tRNA) [8] and

18S ribosomal RNA (rRNA) [9] based on earlier studies, is a highly conserved RNA modification. However, recent research has revealed that ac4C is ubiquitously present in human cells and plays a crucial role in the post-transcriptional regulation of messenger RNA (mRNA) translation and degradation [10, 11]. Furthermore, accumulating evidence suggests that dysregulation of ac4C and its unique writer, N-acetyltransferase 10 (NAT10), significantly contribute to the pathogenesis of various diseases, including cardiomyocyte apoptosis [12], osteoporosis [13], HIV (Human Immunodeficiency Virus) and enterovirus 71 (EV71) replication [14, 15], oocyte development [16] and spermatogonial differentiation failure [17]. Notably, aberrant ac4C modification has been implicated in the progression of several solid tumors, such as bladder cancer [18], gastric cancer [19], colorectal cancer [20] and cervical cancer [21], highlighting the potential of NAT10 as a promising therapeutic target for cancer treatment. Several studies have suggested that NAT10 contributes to the proliferation and metastasis of HCC cells [22–25]. Nevertheless, the precise biological implications and key mechanisms of ac4C modulators in HCC progression remain enigmatic.

As one of the most prevalent mRNA modifications, acetylation peaks were detected in several thousand HeLa cell mRNAs using an antibody-dependent approach, with the majority occurring within the 5′ untranslated regions (5′ UTR) and coding sequences (CDSs) [10, 11]. Acetylation of cytidine in the 5′ UTR has been shown to impede translation initiation, while CDS ac4C modifications are postulated to enhance mRNA translation efficiency [10]. Current understanding suggests that N4-acetyl modification can facilitate hydrogen bonding with guanosine, thereby augmenting interactions with cognate tRNAs and enhancing translation elongation [11]. Despite supporting evidence for the enrichment of ac4C within coding sequences to bolster mRNA decoding efficiency, the precise mechanism by which ac4C promotes mRNA translation remains elusive. It is noteworthy that the biological significance of RNA modification hinges on specific binding proteins that regulate pre-mRNA splicing, mRNA decay, and translation [26]. Consequently, the identification and characterization of ac4C-binding proteins that directly guide distinct bioprocesses assume paramount importance.

In this study, we aimed to investigate the role of NAT10-ac4C and the downstream mechanism in HCC progression. By investigating these factors, our objective was to provide new valuable insights into the mechanisms underlying HCC progression, thereby potentially facilitating the development of novel therapeutic strategies for HCC.

2 | METHODS

2.1 | Patient cohorts and tissues

Tumor tissues were obtained from the surgical specimen archives of 123 HCC patients who had not undergone preoperative treatments at Tongji Hospital of Huazhong University of Science and Technology (HUST, Wuhan, China) between 2012 and 2021. Among them, 20 frozen tissues were utilized for ac4C dot blot, ultra-performance liquid chromatography-tandem mass spectrometry (UPLC-MS/MS), quantitative reverse transcription PCR (qRT-PCR), and western blotting analyses, while 103 formalin-fixed and paraffin-embedded tissues were employed for immunohistochemistry analyses. All patients provided written informed consent, and the study complied with relevant regulations after obtaining approval from the Ethics Committee of Tongji Hospital (HUST, Wuhan, China) (permit number: TJ-IRB20211163).

2.2 | Animal studies

All animal care and studies were performed following the National Institutes of Health Guidelines for the Care and Use of Laboratory Animals and authorized by the Ethics Committee of Tongji Hospital (HUST, Wuhan, China) (permit number: TJH-202110006). All animal models were established according to our previous work [27]. Panobinostat was solubilized in a solution containing dimethyl sulfoxide (DMSO, Sigma-Aldrich, California, USA), PEG300 (Selleck, Texas, USA), Tween 80 and phosphate-buffered saline (PBS) at a ratio of 2:35:2:61 (v/v/v/v). All animal models were randomly assigned to two treatment groups (5mg/kg and 10mg/kg, every other day [qod], intraperitoneal [i.p.]) and vehicle (PBS solution with 2% DMSO, 35% PEG300 and 2% Tween 80, qod, i.p) starting from day 4 after cell implantation. At each final time point, mice were humanely euthanized to obtain tumor samples, and representative tumors were photographed.

2.3 | in vitro cell-behavior assays

For the Cell Counting Kit-8 (CCK-8) assays, 3,000 cells in 100 μL of Dulbecco's Modified Eagle Medium (DMEM, Gibco, USA) were evenly distributed in 96-well plates and incubated over four consecutive days. Cell viability was assessed using a CCK-8 assay from Beyotime Biotechnology (Shanghai, China), following the manufacturer's

protocol. For the wound-healing assays, an optimal density of 1×10^6 cells per well was established in 6-well plates. Confluent monolayers were mechanically disrupted using a 100 μL plastic pipette tip. Healing progress was quantified after 24 or 72 hours by analyzing the area of closure using ImageJ software (National Institutes of Health, USA). For migration and invasion assays, Transwell chambers (Corning, NY, USA) were utilized in 24-well plates containing DMEM supplemented with 10% fetal bovine serum (FBS). Specifically, for invasion assays, the chambers were pre-coated with Matrigel. The ideal seeding density was determined to be 20,000 cells per chamber for migration assays and 50,000 cells per chamber for invasion assays. In the colony formation assays, 1,000 cells were seeded in each well of 6-well plates. After a two-week incubation period, the cells were washed with PBS, fixed with methanol, and stained with 0.05% crystal violet (Servicebio, Wuhan, China). The colony formation rate was calculated as follows: (Number of colonies / Number of seeded cells) × 100%. The number of cells in each chamber was also counted using ImageJ (National Institutes of Health, USA).

2.4 | qRT-PCR

Total RNA was extracted using the Cell Total RNA Isolation Kit (Foregene, Chengdu, China). First-strand complementary DNA (cDNA) synthesis was conducted using the HiScript® III 1st Strand cDNA Synthesis Kit (Vazyme Biotech, Nanjing, China) and random primers. qRT-PCR was carried out employing ChamQ™ SYBR® qPCR Master Mix (Vazyme Biotech, Nanjing, China). All reactions were executed in triplicate. U6 was utilized as an endogenous control. Relative gene expression levels were determined using the comparative Ct ($2^{-\Delta\Delta CT}$) method. All the primer sequences are listed in Supplementary Table S1.

2.5 | Western blot analysis

Total protein was extracted using RIPA Lysis Buffer (Beyotime Biotechnology, Shanghai, China) supplemented with protease inhibitor (MCE, NJ, USA). Protein concentrations were quantified with the BCA Protein Assay Kit (Thermo Fisher Scientific, Massachusetts, USA). Subsequently, proteins were subjected to sodium dodecyl sulfate-polyacrylamide gel electrophoresis (SDS-PAGE) and then transferred onto polyvinylidene fluoride (PVDF) membranes (Millipore, Massachusetts, USA). The membranes were sequentially incubated with primary antibodies and horseradish peroxidase (HRP)-conjugated secondary antibodies, and all the antibodies are listed in Supplementary Table S2. Immunoreactivity was visualized using the enhanced chemiluminescence (ECL) chromogenic substrate (Millipore, Massachusetts, USA). Signal intensities were detected using the ChemiDoc MP Imager System (Bio-Rad, California, USA) and quantified with Image Lab 5.2 software (Bio-Rad, California, USA).

2.6 | small interfering RNA (siRNA), short hairpin RNA (shRNA), and plasmid constructs

RiboBio (Guangzhou, China) designed and synthesized all siRNA, and the siRNA sequences are listed in Supplementary Table S3. NAT10 shRNA and NAT10 cDNA were cloned into lentiviral vector pLKO.1 and pCDH lentiviral vectors (AuGCT, Wuhan, China). The catalytic mutant (aa641, G→E) was constructed based on the wild-type NAT10, and HMGB2 cDNA was cloned into the pCDH vector.

2.7 | Cell culture, transfection, and viral transduction

Huh-7, Hep3B, HepG2 and HEK-293T cell lines were purchased from the China Center for Type Culture Collection (Wuhan, China). HLF was acquired from JCRB cell bank (Tokyo, Japan). MHCC-97H and HCC-LM3 cells were obtained from the Liver Cancer Research Institute of Shanghai Zhongshan Hospital (Shanghai, China). SNU449, SNU182 and SNU387 cell lines were acquired from ATCC (Manassas, VA, USA). Huh7, HEK-293T, MHCC-97H, and HCC-LM3 cell lines were cultured in DMEM. Hep3B and HepG2 cell lines were cultured in Minimum Essential Medium (MEM, Gibco, USA). SNU449, SNU182, and SNU387 cell lines were cultured in Roswell Park Memorial Institute (RPMI) medium (Gibco, USA). According to the manufacturer's protocol, the siRNAs were transfected using GenmuteTM Reagent (SignaGen Laboratories, Maryland, USA). GenJetTM Plus reagent (SignaGen Laboratories, Maryland, USA) was used for cell transfection with plasmids. Virus-containing supernatant was collected 48 h after co-transfection of psPAX2, pMD2G and shRNA-containing, ORF-containing or Luciferase plasmids into HEK293T cells and added to the target cells. 48 h later, infected cells were selected with 1 μg/ml puromycin (MCE, NJ, USA, for the puromycin lentiviral vectors) or 100 μg/mL geneticin (MCE, NJ, USA, for the geneticin lentiviral vector). MHCC-97H cells expressing luciferase (MHCC-97H-luc) were generated as described above. All cells were cultured with 10% fetal bovine serum,

100 U/mL penicillin, and 100μg/mL streptomycin in an incubator with 5% CO_2 at 37°C.

2.8 | Isolation of total and polyadenylated RNA

Total RNA was isolated from HCC tissues and cultured cells using the Total RNA Isolation Kit (Foregene, Chengdu, China) according to the manufacturer's instructions. Subsequently, Turbo™ DNase I treatment (ThermoFisher Scientific, Massachusetts, USA) was performed. Polyadenylated RNA [poly(A) RNA] enrichment was accomplished using the NEBNextR Poly(A) mRNA Magnetic Isolation Module for LC-MS, dot blot, or acetylated RNA immunoprecipitation and sequencing (acRIP-seq), following the manufacturer's instructions. Poly(A) RNA precipitations were carried out using 0.3mol/L sodium acetate [pH 5.5], 15 μg/mL linear acrylamide (ThermoFisher Scientific, Massachusetts, USA) and 2.5× ethanol.

2.9 | Immunohistochemistry (IHC)

Immunohistochemistry (IHC) was performed to measure target protein expression according to our previous study [27]. NAT10 staining was independently assessed by two pathologists blinded to the clinical data. The staining intensity was assessed using a semi-quantitative immunoreactivity score (IRS) as previously reported [28]. Samples with an IRS of 0-6 and 8-12 were classified as having low and high expression of NAT10, respectively.

2.10 | Luciferase reporter assay

Luciferase assay was performed using reporter lysis buffer (catalog #E3971, Promega, Madison, USA) and luciferase assay reagent according to the manufacturer's instructions. Briefly, NAT10 control and NAT10 depleted cells were transfected with pmiRGLO, pmiRGLO-WT-5′ UTR, or pmiRGLO-Mut-5′ UTR in a 12-well plate. After 24 h incubation, cells were analyzed with the Dual-Glo Luciferase Assay system (Promega, Madison, USA). Renilla Luciferase (R-luc) was used to normalize firefly luciferase (F-luc) activity to evaluate reporter translation efficiency.

The CDS sequence of HMGB2 was biosynthesized VectorBuilder (Guangzhou, China) and subcloned into the dual-luciferase vector pmiGLO (Promega, USA). Three putative ac4C recognition sites were identified in CDS. Mutagenesis of ac4C sites (C to T) was performed using a site-directed mutagenesis kit (Thermo Fisher, Massachusetts, USA). Luciferase activity was measured using the Dual-Luciferase Reporter Gene Assay Kit (Promega, Madison, USA). The firefly luciferase activity values were normalized to the Renilla luciferase activity values that reflect expression efficiency. The mRNA abundance was determined as qRT-PCR of F-luc, and the translation efficiency is defined as the quotient of reporter protein production (F-luc/R-luc) divided by mRNA abundance [29]. Experiments were performed three times with similar results.

2.11 | ac4C dot blot assay

The dot blot assay was performed with an anti-ac4C antibody as described previously [11]. Briefly, total RNA or mRNA with denaturation solution were initially denatured at 65°C for 5 minutes, placed on ice for 5 minutes and loaded onto Hybond-N+ membranes, which were then cross-linked. The membrane was washed and incubated with anti-ac4C antibody at 4°C overnight. Then, the membrane was washed and incubated with a secondary antibody for 1 hour at room temperature. Finally, the membrane was visualized using a chemiluminescent HRP substrate. Methylene blue staining was used as the control.

2.12 | mRNA ac4C detection and quantification by UPLC-MS/MS

Briefly, mRNA was extracted and purified from HCC tissues as described above. Briefly, 1μg of mRNA was treated with buffer, S1 nuclease, alkaline phosphatase, and phosphodiesterase I, followed by incubation at 37°C. After the digestion of RNA into nucleosides, the mixture underwent chloroform extraction. The resulting aqueous layer was collected for analysis using a UPLC system (ExionLC™ AD) coupled with an MS System (Applied Biosystems 6500 Triple Quadrupole). The MS system was equipped with an ESI Turbo Ion-Spray interface and controlled by Analyst 1.6.3 software (AB Sciex). The identification and quantification of ac4C modification were performed using the MetWare platform (http://www.metware.cn/) based on the AB Sciex QTRAP 6500 LC-MS/MS platform.

2.13 | Acetylated RNA immunoprecipitation (acRIP)

acRIP was performed as described in a previous publication [11]. Briefly, total RNA was extracted using TRIzol

(Invitrogen, CA, USA) and fragmented by NEBNext® Magnesium RNA Fragmentation buffer or not. Fragmented RNA (10 μg) was immunoprecipitated with 1 μg anti-ac4C or IgG pre-coupled to Protein G Dynabeads 6 hr at 4°C in 100 μL of RIP wash buffer (Millipore, Massachusetts, USA) containing 40U murine RNase inhibitor (Vazyme Biotech, Nanjing, China). Beads were washed five times in RIP wash buffer, and elution of RNA was carried out by RNase-free Proteinase K (50 μg, Millipore, Massachusetts, USA) digestion for 45 minutes at 55°C. The enriched RNAs were extracted by phenol: chloroform: isoamyl alcohol (125: 24: 1) and ethanol precipitation using 0.3 mmol/L sodium acetate (pH 5.5) and 15 μg/mL linear acrylamide. Isolated RNA fragments were subjected to one-step reverse transcription PCR to detect ac4C-modified mRNAs of target genes.

2.14 | acRIP-seq

acRIP-seq was performed by DIATRE Biotechnology (Shanghai, China). Briefly, Poly(A) RNA was isolated by two rounds of oligod(T) selection and fragmented using NEBNext® Magnesium RNA Fragmentation buffer for 5 minutes at 94°C. The anti-ac4C antibody, Dynabeads Protein G (Invitrogen, CA, USA), and purified RNA were incubated at 4°C for 6 hours. The immunoprecipitated RNA was collected according to the above descript (see Acetylated RNA immunoprecipitation). The library was constructed using the NEBNext® Ultra™ Directional RNA Library Prep Kit and then sent for sequencing with the Illumina Nova Seq (Illumina, CA, USA), following the protocol from a company (DIATRE, Shanghai, China). MACS2 identified signal distribution (peak calling). Deeptools generated peak and motif annotation results.

2.15 | RNA sequencing

RNA was extracted and treated with DNase I. After passing quality control, libraries were generated and subjected to sequencing using the Illumina HiSeq 4000 platform (PE150) following the protocol provided by Epibiotek (Guangzhou, China). The RNA-seq reads underwent adapter removal using cutadapt (version 1.18) and were then aligned to the human reference genome (GENCODE, version 30) using HISAT2 (version 2.1.0) with default parameters. The number of reads mapped to each gene was quantified using HTSeq (version 0.11.2) with the "-m intersection nonempty" option. Gene expression levels were determined as fragments per kilobase of transcript per million mapped reads (FPKM) using the DESeq2.12 package [30].

2.16 | Ribosome profiling

The ribosome profiling analyses (Ribo-seq) methodology was followed as described in a previous publication [31]. Prior to collection, cells were treated with 100 mg/mL cycloheximide for 5 minutes at 37°C. Following lysis and RNAse I treatment to degrade unprotected mRNA regions, intact mRNA-ribosome complexes were isolated and sequenced using the Illumina HiSeq 4000 (SE50) protocol provided by Epibiotek. Reads were preceded by removing adapters. The reads that mapped to human ribosomal RNA, small nucleolar RNA, small nuclear RNA, and tRNA from the GENCODE project (version 30) were excluded. The remaining reads were aligned to the human genome using bowtie2 (version 2.3.4.3) with the -L 10 option. The expression levels of protein-coding genes were quantified using featureCounts (version 1.6.4) with parameters including –M and —-fracOverlap set at 0.4 as well as –largestOverlap.

2.17 | Cross-linked RNA immunoprecipitation assays

RNA immunoprecipitation was conducted according to our previous study [27]. Briefly, 0.3% formaldehyde was used to cross-link, and glycine solution was used to quench the cells. After treatment with or without 1 U RNase T1 (Thermo Fisher, Massachusetts, USA) for 15 minutes at 24°C, the cell lysate was utilized to conduct immunoprecipitation in accordance with the manufacturer's protocol of Magna RIP™ RNA-binding Protein Immunoprecipitation Kit (Millipore, Massachusetts, USA). The IP enrichment ratio of a transcript was calculated as the ratio between its abundance to its abundance in the input sample.

2.18 | in vitro transcription of ac4C-containing RNA probes

RNA probes containing ac4C were synthesized following the protocol from Hippo Biotechnology (Huzhou, China). Briefly, in vitro transcription used a DNA template containing the T7 promoter. This RNA oligo used ac4CTP (MCE, NJ, USA) or CTP as the unique source of the C site. After in vitro transcription, synthesized probes were purified by VAHTS RNA Clean Beads (Vazyme, Nanjing, China) according to the manufacturer's instructions.

The purified RNA probes were labeled with biotin using Pierce™ RNA 3' End Biotinylation Kit (Thermo Fisher Scientific, Massachusetts, USA). The RNA probe sequences are listed in Supplementary Table S4.

2.19 | RNA pull-down

The RNA pull-down assay was conducted using the Pierce MagneticRNA-Protein Pull-Down Kit (Thermo Fisher Scientific, Massachusetts, USA) according to the manufacturer's instructions. Briefly, up to 50pmol of ss-C and ss-ac4C probes were mixed with 2mg of protein extract and 50μL of washed streptavidin beads. After incubation for 4 hours at 4°C and three washes, the streptavidin beads were boiled in SDS buffer and used for western blotting.

2.20 | DIA proteomics analysis

The eluted proteins captured by streptavidin beads in ss-C and ss-ac4C were subjected to DIA proteomics quantification according to the protocol from SpecAlly (Wuhan, China). The digested peptides were loaded onto a timsTOF Pro mass spectrometer (Bruker Daltonics) coupled with an UltiMate 3000 RSLC nano-system (Thermo Fisher Scientific, Massachusetts, USA) and analyzed in diaPASEF mode. The raw DIA data were searched against the reviewed human database from UniProt (2020-05-10, 75074 entries) using DIA-NN software (V1.8.1). Proteins with a $|\log2\ FC| > 1$ (fold change > 2 or < 2) and $P < 0.05$ (Student's t-test) were identified as differentially expressed proteins (DEPs). Gene ontology (GO) classification enrichment of DEPs was conducted using the "cluster Profiler" packages (significant at $P < 0.05$).

2.21 | Drug affinity responsive targets stability (DARTS)

DARTS was conducted to the direct binding between Panobinostat and NAT10 in cellular following the published protocol [32]. Briefly, 4×10^7 MHCC-97H cells were lysed in M-PER (Thermo Fisher Scientific, Massachusetts, USA) with protease inhibitor cocktail and phosphatase inhibitor cocktail. TNC buffer (50 mmol/L Tris-HCL pH 8.0, 50 mmol/L NaCl, and 10 mmol/L $CaCl_2$) was added to the lysate, and the protein concentration was determined by BCA assay. Cell lysates were incubated with varying concentrations of Panobinostat or DMSO (vehicle) at room temperature for 1 hour, followed by digestion with Pronase (0.4 μg/mL, 10165921001, Roche) at room temperature for 30 minutes. The digestion was halted using a protease inhibitor cocktail, and the samples were immediately placed on ice. Subsequently, western blotting was used to determine whether NAT10 was a direct target of Panobinostat, while GAPDH served as a negative control.

2.22 | Cellular thermal shift assay (CETSA)

To determine whether Panobinostat (LBH589) acts as a direct ligand of NAT10 protein, CETSA was conducted with intact MHCC-97H as published previously [33]. 1.5×10^7 MHCC-97H cells were collected, washed with ice-cold 1x PBS and subjected to freeze-thaw cycles with liquid nitrogen in the lysis buffer (50 mmol/L Tris-HCl (pH 7.5), 150mmol/L NaCl, and 2mmol/L DTT) plus protease inhibitor cocktail. After centrifugation (20,000 g, 20 minutes, 4°C, Eppendorf), the supernatant was incubated with various concentrations of Panobinostat for 25 minutes and then transferred into the Bio-Rad T100 Thermal Cycler followed by denaturing at indicated temperatures for 3 minutes. Then the samples were centrifuged (20,000 g, 10 minutes, 4°C, Eppendorf), and the supernatant was analyzed by western blotting assay with the NAT10 antibody (Abcam, Cambridge, UK) and GAPDH antibody (Proteintech, Wuhan, China).

2.23 | Surface plasmon resonance (SPR) analysis

SPR analysis was performed using a Biacore x100 system (GE Healthcare Life Sciences, Marlborough, MA, USA) to determine the direct binding between Panobinostat and NAT10 in vitro. NAT10 protein (Origene, Rockville, MD, USA) was immobilized onto a CM7 chip (GE Healthcare Life Sciences, Marlborough, MA, USA) via amine coupling. Panobinostat was diluted with running buffer and subsequently loaded into the samples. Curve fitting was performed using Biacore analysis software to obtain the KD values of Panobinostat for NAT10.

2.24 | Polysome profiling

The polysome profiling was performed according to the bio-protocol database (www.bio-protocol.org/e2126). Briefly, the NAT10 control or depleted MHCC-97H cells (six 100 mm dishes) were washed with ice-cold 1× PBS. After removing the remaining PBS, 2mL PBS with 100 μg/ml cycloheximide (CHX, Selleck, TX, USA) was added to cells and incubated at 37°C for 10 minutes. Then, cells were harvested, and 1 mL of cytoplasmic extract

was layered onto 11 mL of 10%–50% sucrose gradient and centrifuged at 39,000 rpm in a Beckman SW-41Ti rotor for 90 minutes at 4°C. Gradients were fractionated and monitored at an absorbance of 254nm (Brandel, Florida, USA). Collected fractions were subjected to western blot for EEF2 (Abcam, Cambridge, UK), or to RT-PCR analysis of HMGB2 transcript.

2.25 | Surface sensing of translation (SUnSET) assay

The SUnSET assay was performed as previously described to monitor protein synthesis by pausing with puromycin in cells [34]. Briefly, the cells were incubated in a culture medium supplemented with puromycin (2 μg mL^{-1}) for the indicated time periods. Proteins were extracted from the cells, and western blotting was conducted using anti-puromycin (EQ0001, Kerafast, Boston, USA).

2.26 | Virtual screening and molecular docking analysis

A virtual screening method was conducted to identify possible inhibitors for NAT10. The source of the compound database is the FDA National Drug Code Directory, which can be accessed at https://pubchem.ncbi.nlm.nih.gov/. To identify appropriate compounds, we established the following criteria: (1) molecular weight between 108 and 508 to exclude larger molecules; (2) molecular complexity between 100 and 500 to eliminate difficult-to-synthesize compounds; (3) no more than 10 hydrogen bond acceptors and no more than 5 hydrogen bond donors in accordance with Lipinski's rule. The resulting compounds were subjected to a 3D conformational search using RdKit, and the energy of the conformations was calculated by MMFF force field [35]. The input conformation for docking was selected based on the lowest energy conformation. The target protein NAT10 was constructed using AlphaFold [36] predicted structure with residues 913-1025 removed. The target protein NAT10 was constructed based on the AlphaFold predicted structure, with residues 913 to 1025 removed. Virtual screening and docking were performed using Autodock Vina [37], with docking sites set at center_x = -10.72, center_y = 5.99, center_z = -24.64 and size_x = 20, size_y = 20, size_z = 20. Pymol software was utilized for visualizing the complex structures of the top 25 small molecules.

2.27 | Statistical analysis

Statistical analyses were conducted using GraphPad Prism 9.5 software (San Diego, CA, USA). Appropriate tests, including the Student's *t*-test, chi-square test, and Wilcoxon signed-rank test, were performed. X-tile (Yale University, New Haven, CT, USA) weas utilized to determine the optimal cut-off value. Survival curves were assessed using the Kaplan-Meier method, and any differences were evaluated through the log-rank test. Pearson correlation analysis was used to evaluate correlations. Statistical significance was defined as $P < 0.05$.

3 | RESULTS

3.1 | RNA ac4C hyperacetylation and upregulated NAT10 correlate with poor prognosis in HCC

To elucidate the functional roles of ac4C modification in HCC, we initially examined the ac4C RNA levels in 20 HCC tissues and adjacent noncancerous liver tissues. Dot blot assay revealed a significant increase in ac4C levels in HCC tissues total RNA (Figure 1A). This finding was further confirmed by UPLC-MS/MS analysis, which showed a significant elevation in ac4C levels in HCC tissues mRNA (Figure 1B). The observed increase in ac4C levels led us to hypothesize that NAT10, the unique acetyltransferase responsible for ac4C modification, might be dysregulated. Consequently, we compared the mRNA levels of NAT10 in the 20 pairs of HCC and normal liver tissues. Our analysis demonstrated that NAT10 was significantly upregulated in HCC (Supplementary Fig. S1A), and there was a significant correlation between NAT10 expression and ac4C RNA levels in the 20 HCC tissues (Supplementary Fig. S1B-C).

To further validate these results, we performed a large-scale data mining analysis across 89 cohorts of HCC patients. Our investigation revealed notable alterations in NAT10 mRNA levels within 62 of these cohorts. Among them, 54 cohorts of patients showed a significant increase in NAT10 mRNA levels in HCC tissues (Figure 1C). We next performed gene expression analysis using data from The Clinical Proteomic Tumor Analysis Consortium (CPTAC) dataset which supported the upregulation of NAT10 in HCC (Figure 1D). Consistent with these findings, the protein levels of NAT10 were significantly higher in human HCC tissues than in their adjacent noncancerous liver tissues by western blot (Figure 1E). Immunohistochemical analysis of 103 paired samples from an HCC tissue microarray (Tongji cohort) further confirmed the upregulation of NAT10 in HCC samples (Figure 1F). Furthermore, our data indicated that higher NAT10 expression was significantly associated with shorter overall survival and recurrence-free survival times in HCC patients (Figure 1G).

Subsequent analysis showed that high NAT10 expression is significantly associated with advanced clinical

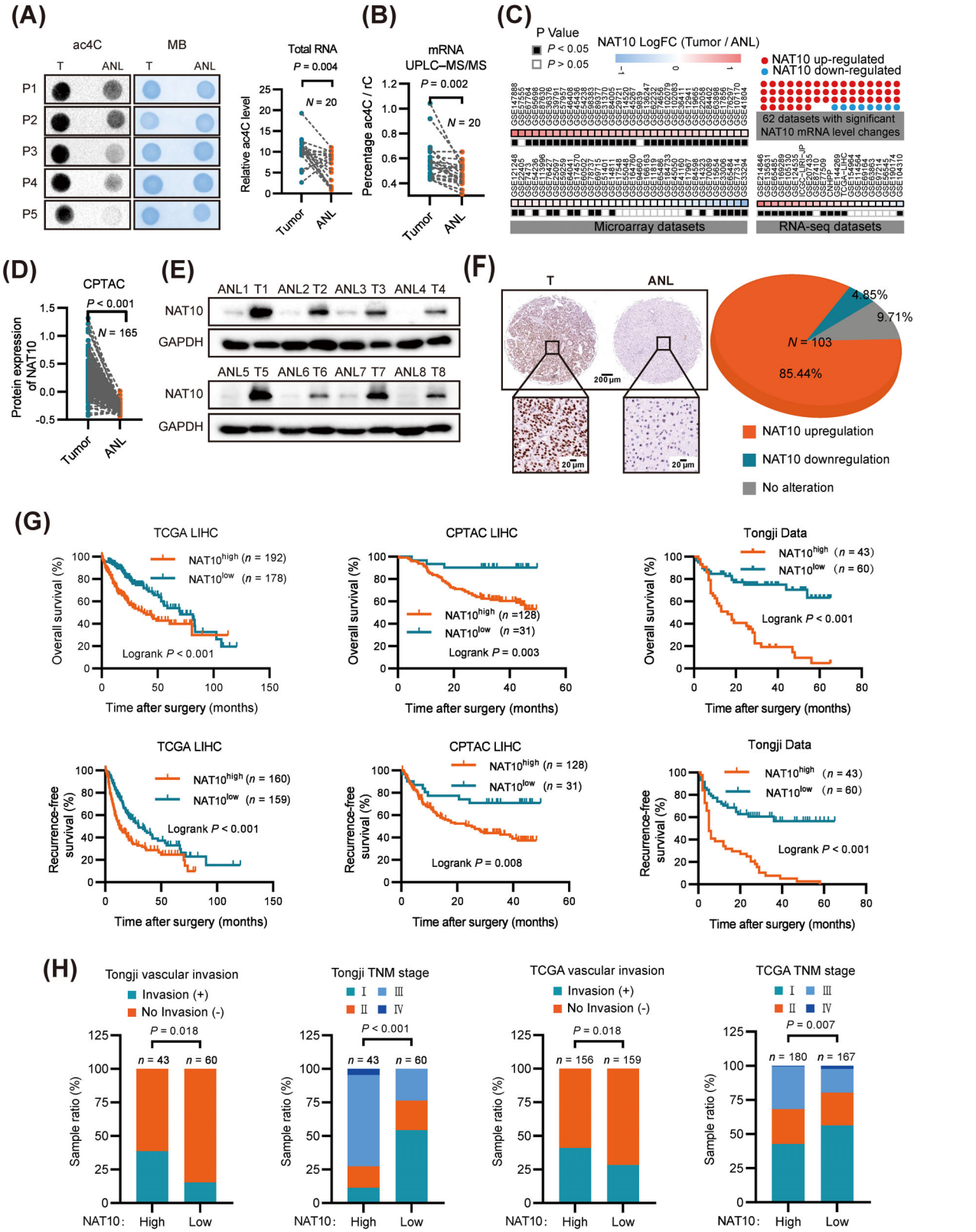

FIGURE 1 Elevated NAT10 expression correlates with poor prognosis in HCC patients. (A) Dot blot analyses of total RNA (5 μg) isolated from HCC tissues and adjacent noncancerous liver tissues using an anti-ac4C antibody, with MB staining as loading control (left panel). Calculation of relative ac4C contents on RNA in HCC tissues and adjacent noncancerous liver tissues (right panel, $N = 20$). (B) Detection of ac4C levels on mRNA in the same 20 HCC tissues and adjacent noncancerous liver tissues by UPLC-MS/MS analysis. (C) Large-scale data mining was used to compare the expression differences in NAT10 mRNA between HCC tissues and adjacent noncancerous liver tissues. (D) Analysis of NAT10 protein levels in HCC and adjacent noncancerous liver tissues ($N = 165$) using CPTAC data. (E) NAT10 protein levels in HCC tissues and adjacent noncancerous liver tissues measured by western blotting ($N = 8$). (F) Representative IHC images of NAT10

stages in patient HCC tissues and iCluster-1 HCC samples, a molecular subtype associated with a poor prognosis [38]. NAT10 expression gradually increases during HCC development (Figure 1H and Supplementary Fig. S1D-I, Supplementary Tables S5-S7). Collectively, these findings suggest that NAT10 expression is closely related to the malignant progression of HCC.

3.2 | Knockdown of NAT10 inhibits HCC proliferation and metastasis

To investigate the function of NAT10 in HCC, we established stable NAT10-knockdown cell lines using cell lines with increased levels of both NAT10 expression and ac4C modification (MHCC-97H and SNU449) (Supplementary Fig. S2A). The knockdown of NAT10 significantly decreased the ac4C content in both total RNAs and mRNAs compared to the non-targeting control shRNA (shCtrl) (Figure 2A). Silencing NAT10 resulted in significant inhibition of HCC cell viability (Figure 2B-C), clonogenic ability (Figure 2D and Supplementary Fig. S2B), and soft agar colony formation efficiency (Figure 2E and Supplementary Fig. S2C). Additionally, the wound healing migration, transwell migration, and matrigel invasion assays revealed that NAT10 silencing significantly suppressed the migration and invasion ability of MHCC-97H and SNU449 cells (Figure 2F-G, Supplementary Fig. S2D-E).

Subsequently, we assessed the effect of NAT10 on HCC proliferation and metastasis in vivo. Tumor xenograft studies showed that silencing NAT10 significantly inhibited tumor growth, as evidenced by reduced tumor size and weight compared to tumors derived from control cells (Figure 2H). Moreover, NAT10 knockdown in tumor xenografts led to inhibited cell proliferation and induced apoptosis, as evidenced by Ki-67 and terminal deoxynucleotidyl transferase-mediated deoxyuridine triphosphate nick-end labeling (TUNEL) staining, respectively (Figure 2I-J). Furthermore, in liver orthotopic-implanted models, the volumes and number of intrahepatic tumor nodules were significantly reduced in the groups inoculated with NAT10 knockdown cells compared to the control group (Figure 2K). Additionally, in a lung metastasis model established by injecting NAT10-knockdown and negative control cells into the lateral tail vein of nude mice, silencing of NAT10 significantly inhibited HCC lung metastasis, as shown by bioluminescence imaging and the number of lung metastatic lesions compared with the control group (Figure 2L).

Taken together, these findings indicate that NAT10 plays a pivotal role as an oncogenic driver in HCC proliferation and metastasis.

3.3 | Effects of NAT10 on ac4C mRNA modification and global mRNA translation

To investigate dysregulated genes involved in ac4C modification in HCC, we performed acRIP-seq in MHCC-97H cells with or without NAT10 knockdown (Figure 3A). The analysis identified a total of 11,591 ac4C peaks from 4,784 ac4C-modified transcripts in control cells and 3,148 peaks from 691 ac4C-modified transcripts in NAT10-deficient cells (Figure 3B-C). Notably, 609 new peaks emerged in stable NAT10 knockdown cells, while 9,052 peaks disappeared. The remaining 2,539 peaks were found in both knockdown and control cells (Figure 3B). As NAT10 is an ac4C acetyltransferase, the 9,052 unique peaks are expected to contain genuine targets of NAT10. The ac4C consensus motif "CXX" was enriched in the detected peaks (Figure 3D), consistent with previous findings [11]. The ac4C distribution patterns within both total and unique peaks were similar in control and NAT10-deficient cells when the RNA species were divided into CDS, 3' UTR, 5' UTR regions of mRNAs, and non-coding RNAs (Figure 3E and Supplementary Fig. S3A). Subsequently, we analyzed the differential ac4C peaks (ratio of normalized ac4C read density [shCtrl/shNAT10], ≥ 2) and their corresponding transcripts by comparing the acRIP-seq data in HCC cells with and without shNAT10. We identified 125 transcripts displaying reduced ac4C peaks in shNAT10 cells (Figure 3F and Supplementary Table S8, collectively indicating that NAT10 mediates ac4C mRNA acetylation in HCC.

It has been reported that ac4C enhances mRNA translation efficiency [11]. Therefore, we conducted RNA-seq and Ribo-seq to identify the downstream functional effectors affected by NAT10-mediated ac4C modification (Figure 3G). NAT10 depletion profoundly alters the gene

expression in the Tongji cohort tissue microarray (TMA) including HCC tissues and adjacent noncancerous liver tissues (left panel); pie chart showing percentages of cases with differential NAT10 expression profiles compared to adjacent noncancerous liver tissues ($N = 103$, right panel, scale bar: 200 μm or 20 μm). (G) Kaplan-Meier plot correlating NAT10 expression with patient overall and recurrence-free survival using CPTAC, TCGA, and Tongji datasets. (H) Analysis of NAT10 expression correlation with malignant features of HCC using Tongji TMA cohort and TCGA LIHC datasets. Statistical tests: (A, B, D) paired t test; (G) log-rank test; (H) Pearson chi-squared test (2-sided).
Abbreviations: ANL, adjacent noncancerous liver tissue; HCC, hepatocellular carcinoma; IHC, immunohistochemistry; LIHC, Liver hepatocellular carcinoma; TCGA, The Cancer Genome Atlas; CPTAC, Clinical Proteomic Tumor Analysis Consortium; MB, methylene blue; ac4C, N4-acetylcytidine; NAT10, N-acetyltransferase 10; mRNA, messenger RNA.

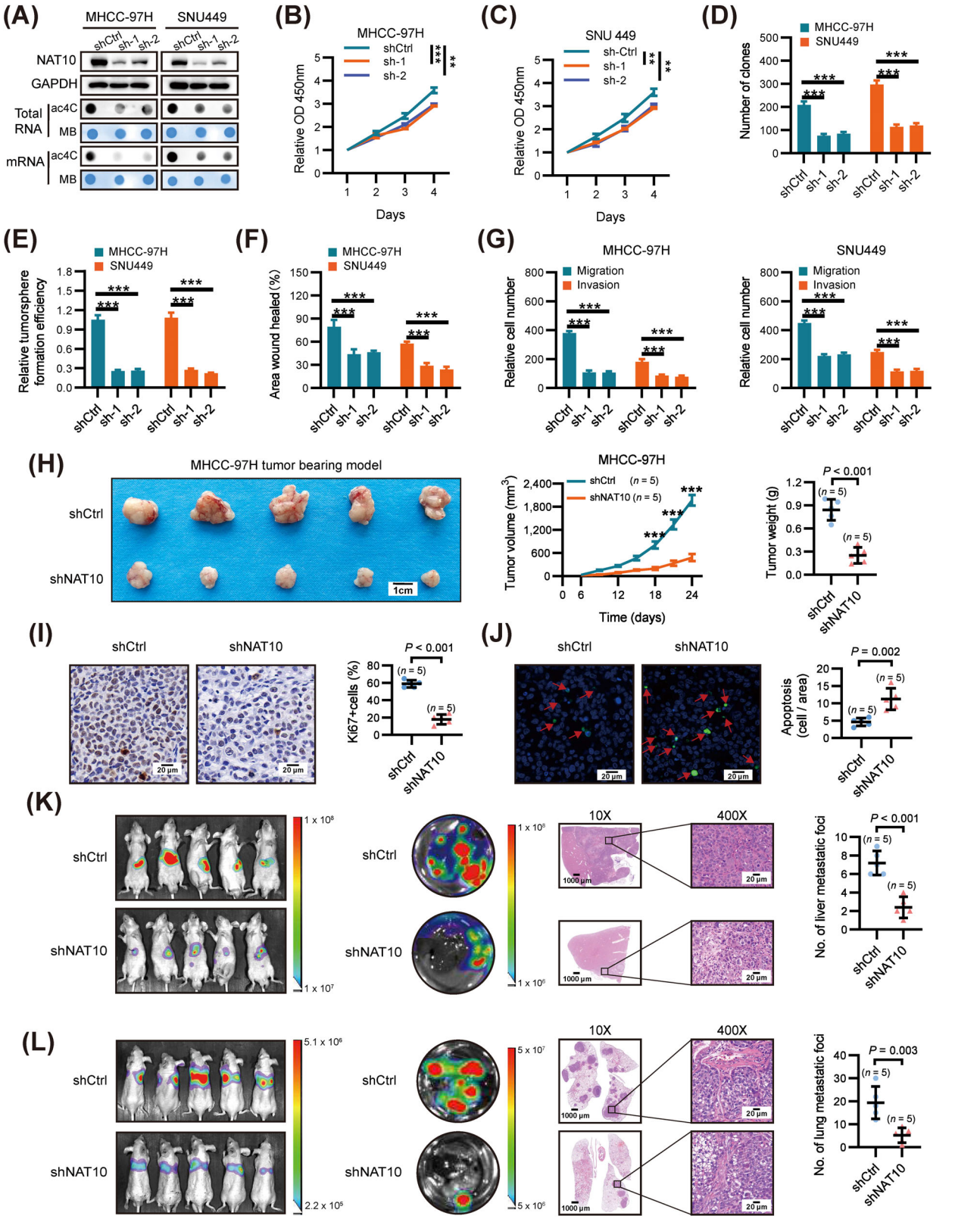

FIGURE 2 NAT10 knockdown inhibits HCC progression in vitro and in vivo. (A) Western blot analysis of NAT10 expression post NAT10 knockdown (upper panel). Dot blot analysis of ac4C levels in total RNA and mRNA isolated from control or NAT10-knockdown HCC cells (lower panel, MHCC-97H and SNU449), with MB staining as loading control. (B) and (C) CCK8 assay for cell viability of NAT10-knockdown and control cells at indicated time points. (D) Colony formation assay quantification for indicated cells. (E) Soft agar colony formation assay quantification for indicated cells. (F) Scratch wound healing assays quantification for indicated cells. (G) Cell migration and invasion assays quantification for MHCC-97H and SNU449 cells. (H) Subcutaneous xenograft models with NAT10-knockdown and control cells ($n = 5$, scale bar: 1 cm). Tumor volume monitored and growth curves generated over 24 days (left panel); tumors weighed (right panel). (I) and (J)

transcriptional expression and ribosome-protected fragment (RPF) abundance (Figure 3H). From RNA-seq, we detected 635 down-regulated and 818 upregulated transcripts upon NAT10 depletion ($P < 0.05$; |log2 fold change| > 1) (Supplementary Table S9). From Ribo-Seq, 277 down-regulated and 332 upregulated transcripts were identified after NAT10 knockdown ($P < 0.05$; |log2 fold change| > 1) (Supplementary Table S10). Comparing translation efficiency (T.E) in MHCC-97H cells with or without NAT10 deletion, we found that ac4C (-) mRNAs displayed elevated T.E specifically in response to NAT10 deletion (Figure 3I and Supplementary Table S11). Next, polysome profiling revealed a significant reduction in the assembly of 80S monosomes and polysomes in NAT10-deficient cells (Figure 3J), indicating that depletion of NAT10 inhibits global protein translation. Furthermore, depletion of NAT10 substantially attenuates protein synthesis, as determined using a SUnSET [34] assay (Figure 3K and Supplementary Fig. S3B). All of these results suggest that NAT10-mediated mRNA ac4C modification enhances global translation efficiency in HCC.

3.4 | NAT10-mediated ac4C modification enhances HMGB2 mRNA translation

To decipher how NAT10 interprets ac4C modifications and modulates mRNA translation in HCC, we employed an integrative approach, overlapping candidate genes identified from acRIP-seq, RNA-seq, and Ribo-seq to pinpoint downstream targets (Figure 4A). Among the potential NAT10 downstream targets (HMGB2, HIF0, PITX1, and STC2), HMGB2 displayed the most significant down-regulation in response to NAT10 depletion (Figure 4B-C), suggesting that HMGB2 could be a direct target of NAT10 in HCC cells. Our acRIP-seq and Ribo-seq data revealed a notable reduction in ac4C enrichment in CDS and ribosome occupancy in NAT10-deficient cells (Figure 4D). Correspondingly, NAT10 knockdown significantly decreased HMGB2 mRNA ac4C levels and protein expression (Figure 4E-F), while its mRNA abundance was unaffected (Supplementary Fig. S4A). Intriguingly, proteasome inhibition using MG132 failed to restore HMGB2 protein expression in HCC cells with NAT10 silencing (Figure 4G), indicating that NAT10-induced HMGB2 expression is not influenced by alterations in protein degradation. Thus, we hypothesized that the downregulation of HMGB2 protein in NAT10-deficient cells might be attributed to differences in translation efficiency. To verify this, we constructed the pmirGLO-HMGB2 luciferase reporter by ligating HMGB2 CDS to the multiple cloning site (MCS). The dual luciferase assay clearly demonstrated significantly lower translation efficiency of HMGB2 in NAT10-deficient cells compared to control cells (Figure 4H, Supplementary Fig. S4B-C). Furthermore, the distribution of HMGB2 mRNAs in the ribosome fractions showed a significant reduction in translation-active polysomes (> 80S) of NAT10-deficient cells compared to control cells (Figure 4I). These collective results indicate that ac4C-induced HMGB2 expression is related to the regulation of translation.

Previous reports have highlighted the crucial role of HMGB2 in promoting HCC progression [39, 40]. Therefore, we conducted rescue assays to confirm the indispensability of HMGB2 in NAT10-induced oncogenic transformation. The overexpression of HMGB2 in NAT10-knockdown cells significantly restored cell proliferation and invasion in vitro (Supplementary Fig. S4D-G). Additionally, in vivo experiments demonstrated that HMGB2 fully rescued the growth of xenografts and lung metastasis following NAT10 knockdown (Figure 4J-L). Our data demonstrated that HMGB2 is a key functional target of NAT10. Furthermore, the clinical relevance of HMGB2 was analyzed in the Tongji and CPTAC cohorts, revealing elevated expression of HMGB2 in HCC tissues (Supplementary Fig. S4H-I). Correlation analysis further revealed a significant association between high expression of HMGB2 and NAT10 levels in HCC (Figure 4M-N). Moreover, survival analysis illustrated that high expression of both genes predicted the poorest overall survival (OS) and recurrence-free survival (RFS) (Supplementary Fig. S4J-K). Together, our findings indicate that NAT10-mediated ac4C modification promotes HCC malignant progression by enhancing HMGB2 translation.

3.5 | CDS ac4C sites of HMGB2 mRNA enhance eEF2 binding

Acetylation of RNA may also affect the binding of interacting proteins, similar to the recognition of

Representative images and quantitative data analysis of Ki67-positive (I) and TUNEL-positive (J) cells, (scale bar: 20 μm). (K) Representative bioluminescence imaging of liver orthotopic implantation models (left panel) and quantification of intrahepatic metastatic nodules (right panel) ($n = 5$). (L) Representative bioluminescence imaging of lung metastasis models (left panel) and quantification of lung metastatic nodules (right panel) ($n = 5$). (B-G) Data shown as mean ± SD, $n = 3$. Statistical analysis: Unpaired t tests. $^{**}P < 0.01$, $^{***}P < 0.001$.
Abbreviations: MB, methylene blue; ac4C, N4-acetylcytidine; NAT10, N-acetyltransferase 10; GAPDH, Glyceraldehyde-3-phosphate dehydrogenase; TUNEL, terminal deoxynucleotidyl transferase–mediated deoxyuridine triphosphate nick-end labeling; CCK-8, Cell Counting Kit-8; SD, standard deviation.

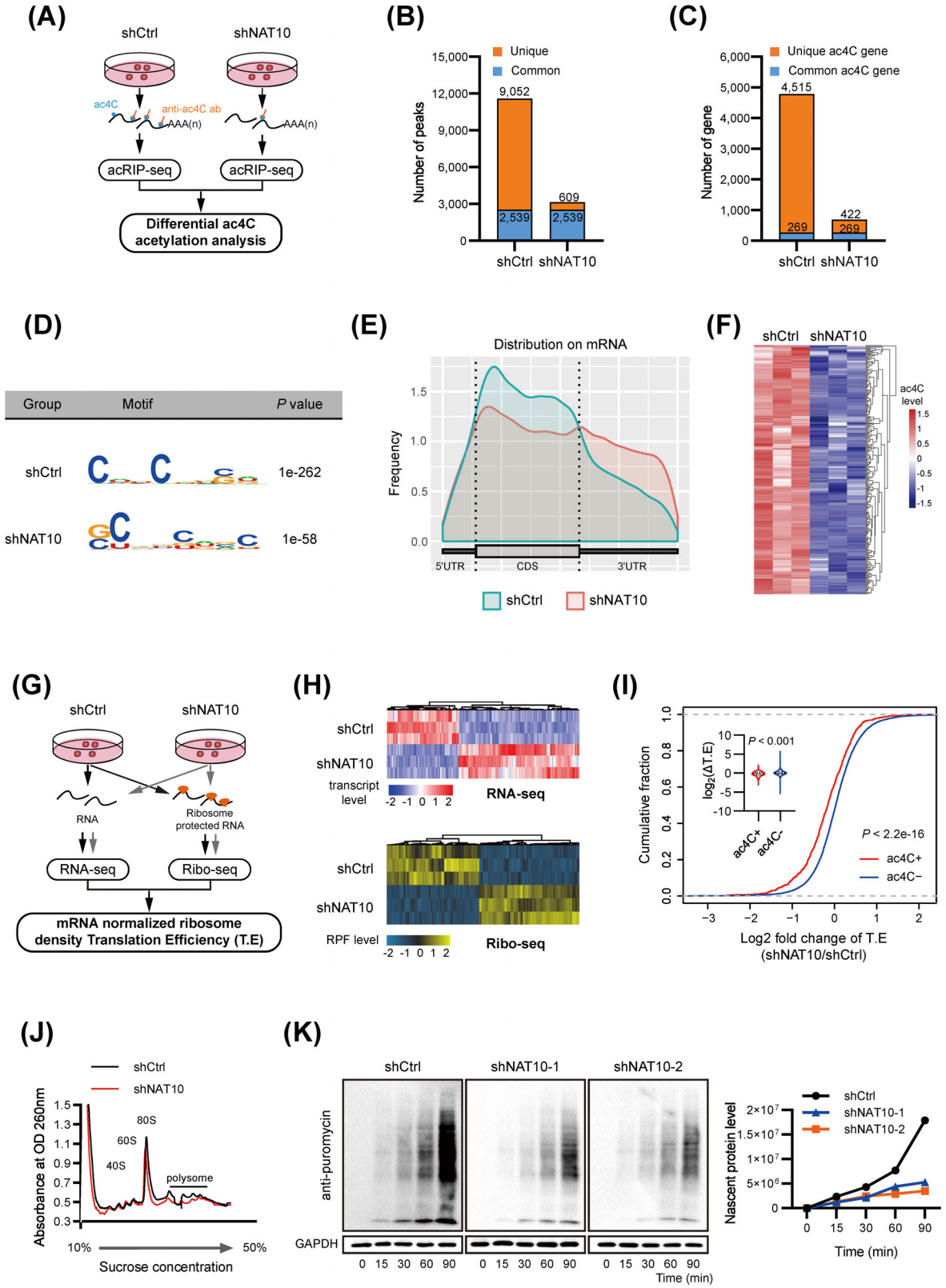

FIGURE 3 Effects of nat10 on ac4c mRNA modification and global mRNA translation. (A) Flow chart depicting acRIP-seq. (B) Number of ac4C peaks identified in acRIP-seq in shCtrl and shNAT10 MHCC-97H cells. (C) Number of ac4C-modified genes identified in acRIP-seq. Common ac4C genes have ≥ 1 common ac4C peak, while unique ac4C genes have no common ac4C peaks. (D) Top consensus motif identified by HOMER with acRIP-seq peaks in MHCC-97H cells with or without NAT10 knockdown. (E) Normalized distribution of ac4C peaks on mRNA in shCtrl and shNAT10 MHCC-97H cells. (F) Heatmaps of 125 transcripts displaying reduced ac4C peaks in shNAT10 cells. (G) Flow chart depicting RNA-seq and Ribo-seq. (H) Heatmaps of transcript level (RNA-seq) and RPF abundance (Ribo-seq). (I) Cumulative distribution of log2-fold changes of mRNA-normalized ribosome footprint reads (T.E) for ac4C(−) and ac4C(+) transcripts in shCtrl and

N6-methyladenosine in RNA by specific binding proteins that mediate mRNA translation [41, 42]. To identify the proteins directly binding to ac4C modifications, we conducted RNA affinity chromatography and data-independent acquisition (DIA) proteomics quantification using biotin-labeled oligonucleotides with or without ac4C for an unbiased screen (Figure 5A-B). As a result, 123 proteins were detected with a log2 ratio of ss-ac4C/ss-C ≥ 1 and P value ≤ 0.05 in the ss-ac4C group (Supplementary Table S12). Gene ontology analysis (GO) showed that the identified proteins were mainly enriched in translation elongation and translation, etc. (Figure 5C and Supplementary Fig. S5A). Additionally, the identified proteins were searched against the STRING protein-protein interaction (PPI) database for known PPIs, and the protein nodes were grouped based on their known functions acquired through GO analysis (Supplementary Fig. S5B). These proteins were divided into six major sub-clusters based on their known biological functions, including translation, targeting to ER, Ribonucleoproteins, etc. All of these results suggest that ac4C modification is involved in translation.

Previous studies have demonstrated that ac4C on the coding sequence of FUS enhances translation efficiency without affecting mRNA levels [11]. Xiang et al. (2021) performed RNA affinity chromatography and mass spectrometry (MS) analyses using biotin-labeled FUS CDS oligonucleotides with or without ac4C from HEK 293T lysates [43]. In an effort to identify specific ac4C-binding proteins responsible for translation, we performed an overlap analysis of ss-ac4C and acFUS binding proteins, which led to the identification of eEF2 and SRP68 (Figure 5D-E). RNA pull-down assays validated that eEF2 and SRP68 preferably bind to ac4C-modified oligonucleotides (Figure 5F). Subsequently, to ascertain the involvement of eEF2 or SRP68 in the regulation of HMGB2 translation, we initially assessed HMGB2 expression through transient siRNA-mediated knockdown of eEF2 and SRP68 (Supplementary Fig. S5C). The findings revealed a significant downregulation of HMGB2 protein upon eEF2 depletion. Further, RNA pull-down assays confirmed that eEF2 indeed showed a much higher binding ability to ac4C-modified RNA (Figure 5G). This indicates that eEF2 is a specific binding protein of ac4C acetylated mRNA.

Additionally, RNA immunoprecipitates (RIP) of endogenous eEF2 showed significant enrichment of ac4C modifications in eEF2-bound RNA (Supplementary Fig. S5D). Moreover, NAT10 depletion correspondingly decreased the distribution of eEF2 in 80S and polysomes (Supplementary Fig. S5E), providing support for the notion that eEF2 serves as an ac4C recognizer. To verify whether eEF2 participates in ac4C acetylation of HMGB2 mRNA, RIP-qPCR was used to investigate the interaction between HMGB2 mRNA and eEF2. Our data showed that eEF2 was significantly enriched in HMGB2 mRNA, and this relative enrichment was significantly suppressed in NAT10-deficient cells (Figure 5H). Overexpression of NAT10 resulted in an upregulation of HMGB2 protein expression, which was significantly attenuated upon eEF2 knockdown (Figure 5I). These findings indicate that eEF2 is involved in the ac4C modification-regulated HMGB2 expression.

To further investigate the acetylation site of HMGB2 mRNA, we employed an ac4C antibody to immunoprecipitate fragmented RNA from HCC cells with or without NAT10 deficiency (Figure 5J). The results revealed that ac4C is predominantly enriched in HMGB2 exon 1/2/3 and the 5′ UTR rather than the 3′ UTR. Interestingly, ac4C enrichment in exon 2, exon 3 and the 5′ UTR was significantly reduced in NAT10-deficient cells, while no similar effect was observed in exon 1 (Figure 5J). Supporting this, we identified one "CXX" motif in the 5′ UTR and three in exon 2 and exon 3 of HMGB2 mRNA (Supplementary Fig. S5F). To explore the potential role of ac4C acetylation in the HMGB2 5′ UTR region, we generated luciferase reporters containing firefly luciferase, followed by either the wild-type HMGB2 5′ UTR or a mutant 5′ UTR (C residues were mutated to T in CXX-rich regions). The HMGB2 5′ UTR-reporter luciferase assay revealed no significant translational difference between control and NAT10-deficient cells for both WT-5′ UTR and mutant-5′ UTR constructs (Supplementary Fig. S5G). Next, we examined whether the three ac4C acetylation sites in the CDS can regulate the expression and translation of HMGB2. For this purpose, we first generated an expression construct containing only the wild-type HMGB2 CDS. Additionally, we constructed three mutant-type HMGB2 CDS variants (mutant1/2/3) by introducing C to T mutations in the CXX-rich regions (Supplementary Fig. S5H). Surprisingly, our data demonstrated that the HMGB2 protein level was almost completely restored in all three types of mutants (Figure 5K). To further support this finding, we mutated the pmirGLO-HMGB2 luciferase reporter accordingly and performed dual-luciferase assays, which showed that all three types of mutants attenuated

shNAT10 MHCC-97H cells (Kolmogorov-Smirnov test or two-tailed t-test). (J) Polysome profiling of shCtrl and shNAT10 MHCC-97H cells. (K) Western blot images of SUnSET assays quantifying nascent (puromycin-labeled) peptides in shCtrl and shNAT10 MHCC-97H cells. GAPDH used as loading control. Abbreviations: acRIP-seq, acetylated RNA immunoprecipitation and sequencing; RNA-seq, RNA sequencing; Ribo-seq, ribosome profiling analyses; T.E, translation efficiency; ac4C, N4-acetylcytidine; NAT10, N-acetyltransferase 10; GAPDH, Glyceraldehyde-3-phosphate dehydrogenase; RPF, ribosome protected fragment; SD, standard deviation.

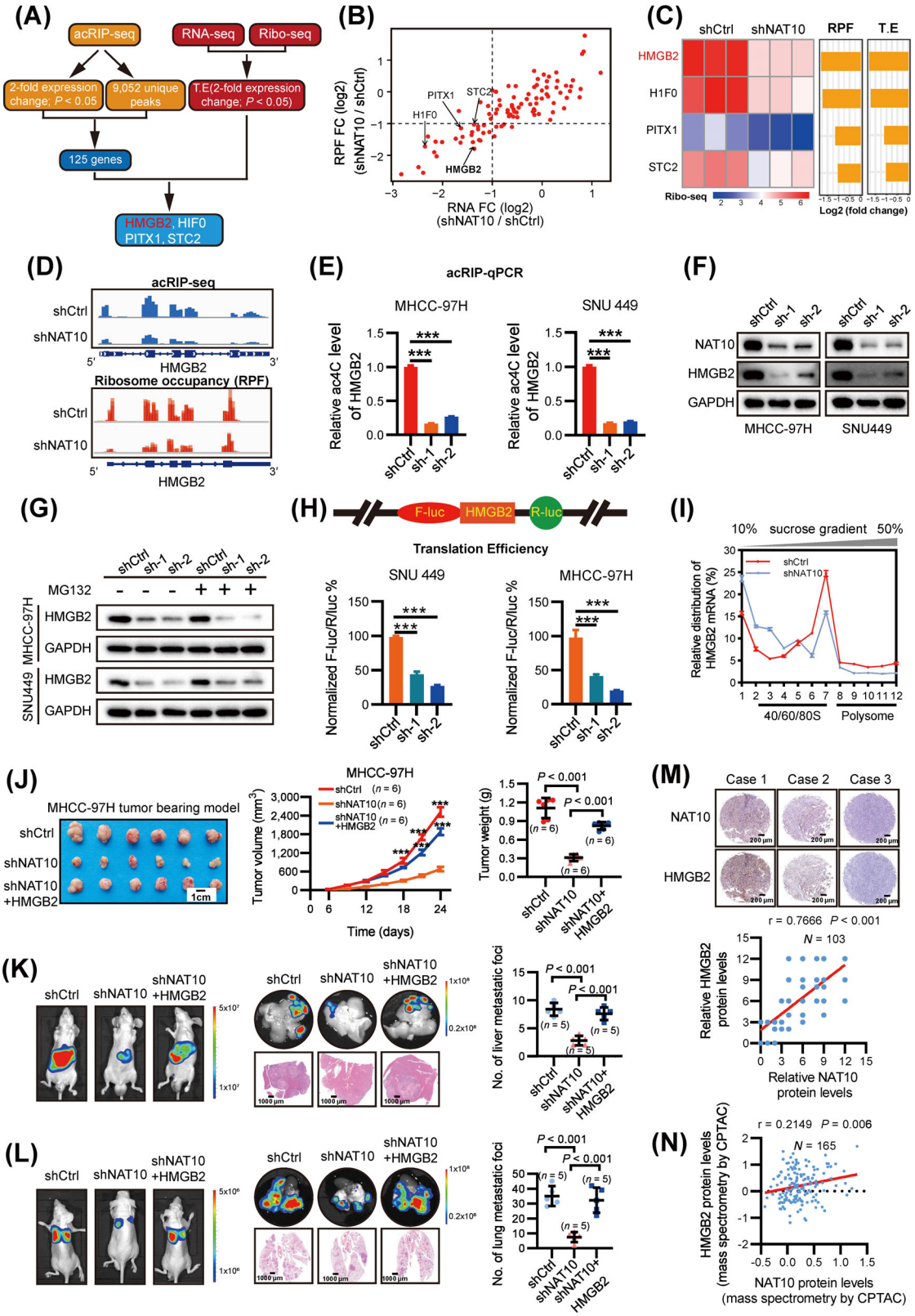

FIGURE 4 ac4C modification enhances translation of HMGB2. (A) Schematic diagram of the strategy for pinpointing key NAT10 targets in HCC. (B) Fold changes of transcript level (RNA-seq) and RPF abundance (Ribo-seq) of 4 downstream targets. (C) Heatmap of RPF abundance for downstream 4 target genes and rank in ordered NAT10 targets gene list using RPF and T.E fold changes. (D) ac4C (top) and RPF (bottom) abundances on HMGB2 mRNA transcripts in shCtrl and shNAT10 MHCC-97H cells. (E) acRIP-qPCR analysis for indicated cells. (F) Western blot of HMGB2 protein expression in NAT10-deficient cells. (G) HCC cells were treated with 10 μmol/L MG132 for 12 hours. (H) NAT10-deficient or control cells transfected with pmirGLO-HMGB2 reporter for 24 h, and HMGB2 translation efficiency defined as reporter protein production (F-luc/R-luc) divided by mRNA abundance [29]. (I) Relative mRNA distribution of HMGB2 in ribosome fractions

NAT10-suppressed translation of HMGB2 (Figure 5L and Supplementary Fig. S5I). Taken together, our data strongly indicate that acetylation in HMGB2 exon 2 and exon 3 is the key site for ac4C-regulated translation of HMGB2 mRNA.

To verify whether eEF2 participates in the three identified ac4C acetylation sites of HMGB2 mRNA, we conducted RIP-qPCR to investigate the interaction between HMGB2 mRNA and eEF2. The results of RIP-PCR revealed that eEF2 predominantly interacts with the identified acetylation CDS region of HMGB2 mRNA rather than the 5′ UTR region (Figure 5M). This interaction was further confirmed through RNA pull-down experiments, which verified the binding of eEF2 to the acetylation CDS region of HMGB2 (Figure 5N). These data strongly suggest that eEF2 is likely responsible for the ac4C-induced translation of HMGB2 mRNA in HCC cells.

3.6 | Identification and characterization of Panobinostat as a NAT10-mediated ac4C inhibitor

Remodelin has been proposed as a potential inhibitor of NAT10, but recent studies have not provided conclusive evidence regarding its inhibitory effect on NAT10-mediated ac4C modification [44]. Consistent with previous findings, our results demonstrate that Remodelin exhibits no significant inhibition of HCC cell ac4C modification and does not modulate the expression of HMGB2 (Supplementary Fig. S6A). This suggests that Remodelin may not be a specific chemical inhibitor of RNA acetylation catalyzed by NAT10. To investigate whether NAT10-promoted malignant phenotypes depend on its ac4C catalytic activity, we constructed plasmids expressing wild-type NAT10 or its catalytic mutant (G641E), which is known to impair the RNA acetyltransferase function of NAT10 [15, 45]. Our analysis revealed a substantial decrease in the ac4C level in cells expressing the catalytic mutant NAT10 compared to wild-type cells (Figure 6A). Importantly, we found that the ac4C catalytic activity domain of NAT10 (G641) is indispensable for its role in promoting the proliferation and invasion of HCC cells (Supplementary Fig. S6B-C). Furthermore, the overexpression of the catalytic mutant NAT10 significantly attenuated protein synthesis (Supplementary Fig. S6D). Meanwhile, we observed that overexpression of the catalytic mutant NAT10 had no effect on HMGB2 protein levels or mRNA ac4C levels (Figure 6A and Supplementary Fig. S6E).

In our efforts to identify potential NAT10 inhibitors, we conducted a structure-based virtual screening to dock FDA-approved drugs to NAT10's catalytic pocket. From the top 25 compounds with high docking scores to the glycine-641 catalytic pocket, we further screened three compounds exhibiting anti-tumor activity from the PubChem database (Supplementary Table S13). Notably, Panobinostat emerged as a promising candidate, exhibiting potent inhibitory effects on RNA acetylation in the initial screen (Figure 6B). As a result, we focused on Panobinostat for further studies. Our docking models suggested that Panobinostat binds tightly to NAT10 protein and blocks its catalytic pocket (Figure 6C and Supplementary Fig. S6F). Subsequently, surface plasmon resonance assays (Figure 6D and Supplementary Fig. S6G) showed a high binding affinity between Panobinostat and NAT10 (KD = 8.544 μM). Additionally, Panobinostat treatment resulted in significant shifts in the thermal stability of NAT10 protein (Figure 6E), indicating its capability to bind to NAT10. The drug affinity responsive target stability (DARTS) assay further confirmed their direct interactions (Figure 6F).

Given the strong interaction between Panobinostat and NAT10, it is plausible that Panobinostat exerts regulatory effects by inhibiting ac4C modification of its target RNAs. Dot blot analysis demonstrated that Panobinostat treatment notably decreased global ac4C abundance in both total RNA and mRNA in a dose-dependent manner (Figure 6G-H). Furthermore, Panobinostat treatment significantly attenuated protein synthesis and inhibited the expression of HMGB2 (Figure 6I). Moreover, Panobinostat led to a significant decrease in HMGB2 mRNA ac4C levels (Figure 6J) and HMGB2 translation efficiency (Figure 6K and Supplementary Fig. S6H) in HCC cell. Additionally,

analyzed by qRT-PCR in shCtrl and shNAT10 MHCC-97H cells. (J) Subcutaneous xenograft model transplanted with indicated cells ($n = 6$, scale bar: 1 cm). Tumor volume monitored and growth curves generated over 24 days (left panel); tumors weighed (right panel). (K) Liver orthotopic implantation models transplanted with indicated cells (scale bar: 1,000 μm). Representative bioluminescence imaging of mice (left panel) and quantification of tumor nodules (right panel) ($n = 5$). (L) Lung metastasis model transplanted with indicated cells (scale bar: 1,000 μm). Representative bioluminescence imaging of mice (left panel) and quantification of lung metastatic nodules (right panel) ($n = 5$). (M) Representative images of NAT10 and HMGB2 protein expression in HCC tissue arrays ($N = 103$) by IHC (upper panel). Pearson correlation analysis between NAT10 and HMGB2 protein expression (lower panel). (N) Pearson correlation analysis between NAT10 and HMGB2 protein expression using CPTAC LIHC dataset. (E) and (H) Data are shown as mean ± SD, $n = 3$. Statistical analysis: Unpaired t-tests. $^{*}P < 0.05$, $^{**}P < 0.01$, $^{***}P < 0.001$. Abbreviations: ac4C, N4-acetylcytidine; NAT10, N-acetyltransferase 10; GAPDH, Glyceraldehyde-3-phosphate dehydrogenase; CPTAC, Clinical Proteomic Tumor Analysis Consortium; qRT-PCR, quantitative real-time polymerase chain reaction; RNA-seq, RNA sequencing; Ribo-seq, ribosome profiling analyses; T.E, translation efficiency; acRIP, acetylated RNA immunoprecipitation; HMGB2, High Mobility Group Protein B2; IHC, immunohistochemistry; SD, standard deviation.

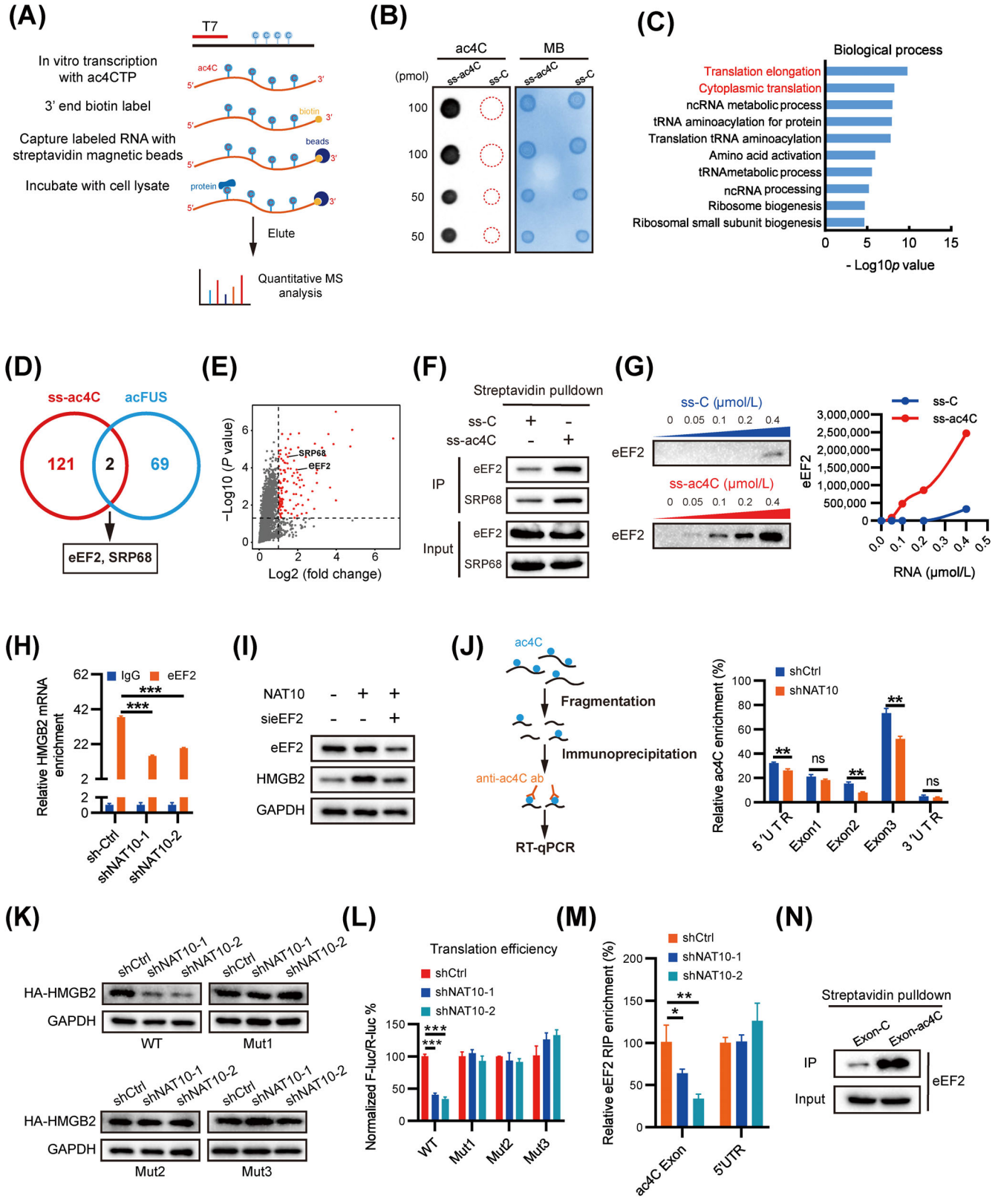

FIGURE 5 CDS ac4C sites of HMGB2 mRNA enhance binding of eEF2. (A) Schematic of RNA affinity chromatography and MS analysis. (B) Dot blot showing ac4C levels (left) and MB (right, loading controls) in ac4C/C ssRNA probes. (C) GO biological process analysis of proteins identified in quantitative MS via the Database for Annotation, Visualization, and Integrated Discovery. (D) Venn diagram comparing proteins identified in ss-ac4C and acFUS. (E) Volcano plot of identified proteins. Proteins significantly enriched in ss-ac4C RNA are shown as red dots. Log2 fold change plotted on x-axis; -log10 P value on y-axis. (F) Western blot images of endogenous eEF2 and SRP68 proteins pulled down by biotin-labeled C-Oligos and ac4C-Oligos from MHCC-97H whole cell lysates. (G) RNA pull-down assays showing dose-dependent interaction between endogenous eEF2 and biotin-labeled C-Oligos (top) or ac4C-Oligos (below). Gray signal of bands in

our data showed that eEF2, enriched in HMGB2 mRNA, was significantly suppressed in Panobinostat-treated cells (Figure 6L). These findings collectively indicate that Panobinostat exhibits selective binding to and occupancy of the catalytic pocket of NAT10, thereby inhibiting ac4C modification in target RNA transcripts.

3.7 | Panobinostat exhibits anti-HCC efficacy in vitro and in vivo

To investigate the potential anti-HCC effects, we comprehensively evaluated the impact of Panobinostat on HCC cells in vitro. Notably, Panobinostat demonstrated a dose-dependent inhibition of MHCC-97H cell growth (Figure 7A), with a half-maximal inhibitory concentration (IC50) of 4.469 nmol/L Consistent with NAT10 knockdown, Panobinostat significantly suppressed cell proliferation and invasion (Figure 7B-C). Subsequently, we assessed Panobinostat's anti-HCC role in vivo (Figure 7D), where it did not induce any reduction in body weight (Supplementary Fig. S7A-C). In the subcutaneous xenograft model, Panobinostat effectively inhibited the growth of xenograft tumors in a dose-dependent manner (Figure 7E). To further validate the inhibition effect of NAT10-mediated ac4C in vivo, we examined RNA ac4C levels and HMGB2 protein expression in xenograft tumor tissues from Panobinostat-treated and control mice using dot blot and Western blot, respectively. Panobinostat-treated mice exhibited a significant decrease in ac4C levels in RNA compared to the control mice (Figure 7F). Moreover, Panobinostat effectively inhibited the protein expression of HMGB2 in mice (Figure 7G). Histopathological examination further confirmed Panobinostat's efficacy by demonstrating its inhibitory effect on NAT10 and HMGB2 expression in vivo (Figure 7H). Additionally, the Panobinostat-treated group exhibited a remarkable reduction in both the volumes and the number of intrahepatic tumor nodules compared to the control group (Figure 7I). Notably, Panobinostat treatment significantly inhibited HCC cell lung metastasis, as evidenced by bioluminescence imaging and the quantification of lung metastatic lesions compared to the control groups (Figure 7J). Collectively, these data suggest that Panobinostat is an effective and safe leading compound targeting NAT10-mediated ac4C for potential HCC treatment.

4 | DISCUSSION

In this study, we have demonstrated a significant increase in ac4C modification due to the upregulation of the acetyltransferase NAT10 in HCC. Our findings have established a causal relationship between NAT10-mediated ac4C modification and the promotion of HCC malignancy progression. Additionally, we have identified HMGB2 as the primary target of NAT10-mediated ac4C modification in HCC. Mechanistically, our results reveal that eEF2 preferentially binds to the CDS ac4C motif "CXX", thereby promoting HMGB2 translation elongation. Furthermore, we have identified a potent NAT10 inhibitor, Panobinostat, which effectively inhibits the malignancy progression of HCC. These results collectively highlight the promising therapeutic potential of targeting the NAT10-ac4C/eEF2-HMGB2 axis in HCC (Figure 7K).

Previous reports have emphasized the significance of ac4C modification in the progression of various cancers [46, 47]. As the only known ac4C "writer" protein, NAT10 possesses both acetyltransferase and RNA-binding activities, contributing to enhanced stability and translation efficiency of mRNA [11]. Recent studies have reported that aberrant expression of NAT10/ac4C promotes the progression of several solid tumors, including bladder cancer [48], gastric cancer [49], colorectal cancer [50] and cervical cancer [21]. Consistent with these findings, our study reveals that elevated NAT10 expression induces an increase in ac4C modification in HCC. Moreover, patients with

Western blots (left) quantified by Image Master Total Lab (right). (H) RIP-qPCR analysis of enrichment of HMGB2 mRNA on eEF2 relative to IgG in shCtrl and shNAT10 MHCC-97H cells. (I) Western blot analysis of HMGB2 expressions in Huh7 cells co-transfected with NAT10 CDS plasmid or eEF2 siRNA. (J) Schematic representation of acRIP-qPCR with fragmented RNA from cells (left). ac4C in HMGB2 mRNA analyzed by acRIP-qPCR using fragmented RNA in MHCC-97H cells with shCtrl and shNAT10 (right). (K) Western blot analysis on HA-HMGB2 in MHCC-97H cells seeded in 6-well plates and transfected with either wild-type HMGB2 CDS or mutant1/2/3 HMGB2 CDS plasmid, along with control or NAT10-deficient cells. (L) NAT10-deficient or control cells transfected with either wild-type HMGB2 CDS or mutant1/2/3 HMGB2 CDS reporter for 24 h, and the quotient of reporter protein production defines translation efficiency of HMGB2. (M) Binding of eEF2 with CDS or 5′ UTR in control or NAT10-deficient cells analyzed by eEF2 RIP-qPCR using fragmented RNA. (N) Western blotting showing endogenous eEF2 proteins pulled down by biotin-labeled exon-C RNA and exon-ac4C RNA from MHCC-97H whole cell lysates. (H, J, L-N) Data are shown as mean ± SD, $n = 3$. Statistical analysis: Unpaired t-tests. $^{*}P < 0.05$, $^{**}P < 0.01$, $^{***}P < 0.001$.
Abbreviations: MS, mass spectrometry; ac4C, N4-acetylcytidine; MB, methylene blue; GO, Gene ontology analysis; RIP, RNA immunoprecipitates; NAT10, N-acetyltransferase 10; HMGB2, High Mobility Group Protein B2; eEF2, eukaryotic Elongation Factor 2; CDS, coding sequence; UTR, untranslated regions; acRIP, acetylated RNA immunoprecipitation; SD, standard deviation.

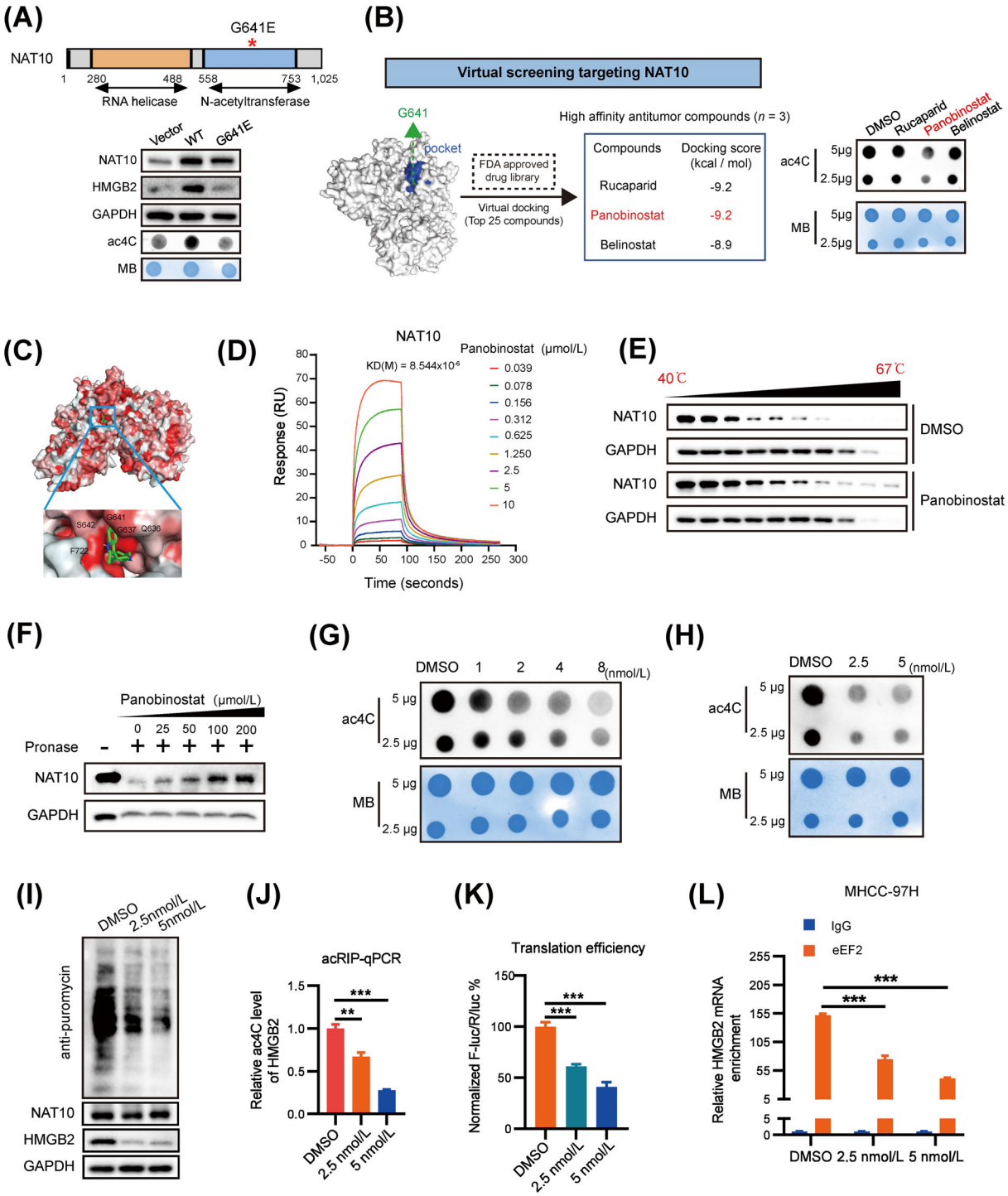

FIGURE 6 Characterization of the NAT10 inhibitor panobinostat. (A) Western blot and dot blot were used to detect HMGB2 expression and ac4C levels after transfection of NAT10 (WT) or G641E NAT10 mutant plasmid, respectively. (B) Flow diagram of NAT10 inhibitor screening. (C) Three-dimensional (3D) binding model of Panobinostat in NAT10 catalytic pocket. (D) Biacore analysis revealing binding between NAT10 protein and Panobinostat. (E) Western blots for effects of Panobinostat on thermal stabilization of NAT10 protein. CETSA assayed in cell lysates. (F) Identification of direct binding between Panobinostat and NAT10 via DARTS assays. (G) Effects of various concentrations of Panobinostat on global ac4C modification in MHCC-97H cells. Dot blot assays were conducted with total RNA. (H) Effects of various concentrations of Panobinostat on poly(A)+ RNA ac4C modification in MHCC-97H cells. (I) Effects of Panobinostat on levels of nascent (puromycin-labeled) peptides and expression of HMGB2. (J) Effects of Panobinostat on HMGB2 mRNA ac4C level using acRIP-qPCR. (K) Effects of Panobinostat on HMGB2 mRNA translation efficiency. (L) RIP-qPCR analysis was performed to determine the enrichment of HMGB2 mRNA on eEF2 relative to IgG in both control and Panobinostat-treated cells. (J-L) Data is shown as mean ± SD, $n = 3$. Statistical analysis: Unpaired t-tests. $^{**}P < 0.01$, $^{***}P < 0.001$. Abbreviations: WT, wild type; ac4C, N4-acetylcytidine; NAT10, N-acetyltransferase 10; HMGB2, High Mobility Group Protein B2; eEF2, eukaryotic Elongation Factor 2; RIP, RNA immunoprecipitates; DARTS, drug affinity responsive targets stability assay; CETSA, cellular thermal shift assay; SD, standard deviation.

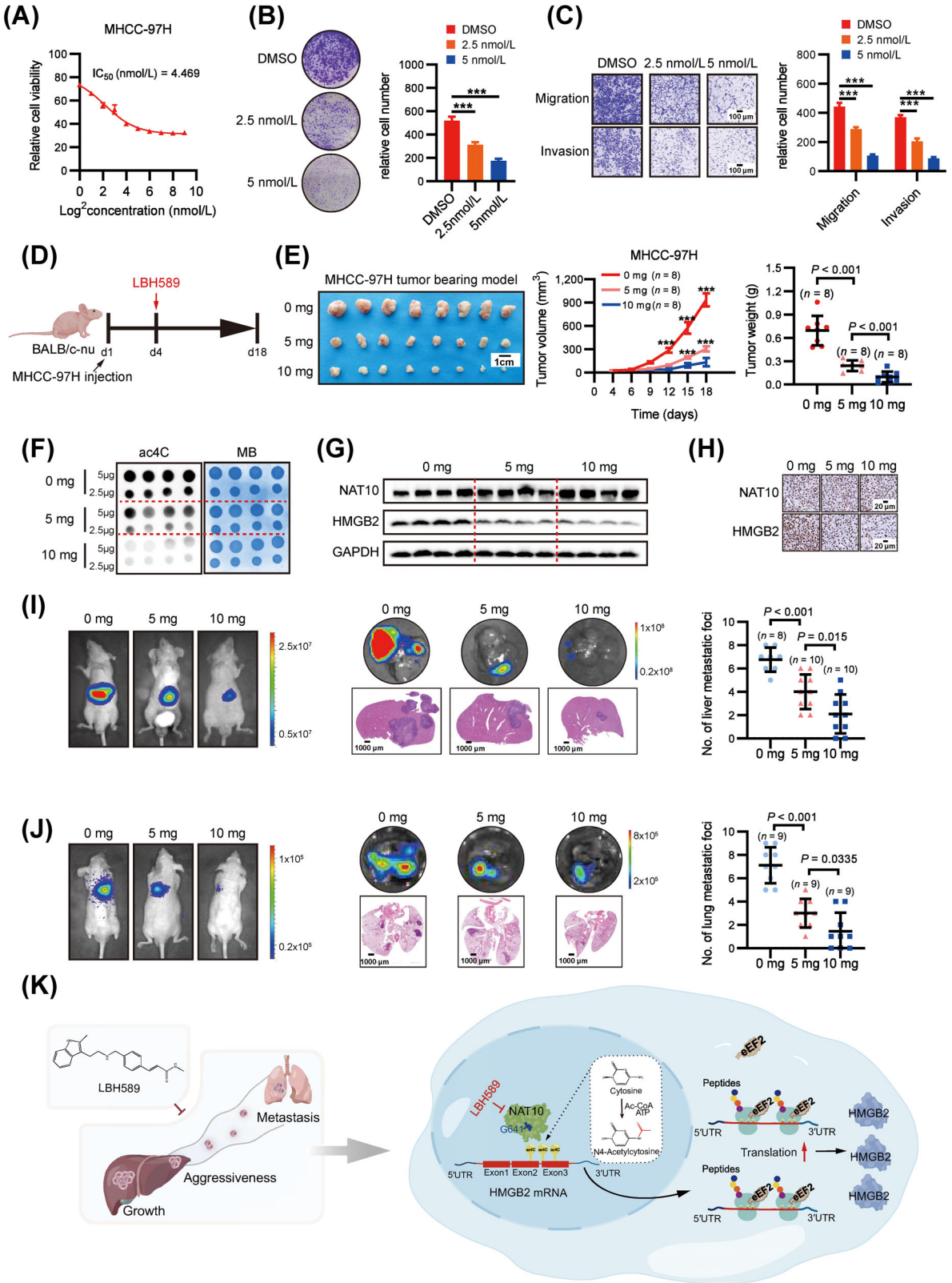

FIGURE 7 Panobinostat exhibits promising anti-HCC efficacy in vitro and in vivo. (A) IC50 values of Panobinostat in MHCC-97H after 48 h of treatment. (B) Effects of various concentrations of Panobinostat on colony formation abilities of MHCC-97H cells. (C) Effects of various concentrations of Panobinostat on cell migration and invasion abilities of MHCC-97H cells (scale bars = 100 μm). (D) Schematic diagram of generation and treatment of HCC models in mice. (E) Effects of different concentrations of Panobinostat on tumor volume and weight of subcutaneous xenograft model ($n = 8$, scale bar: 1 cm). (F) Effects of various concentrations of Panobinostat on ac4C level in subcutaneous xenograft model. (G) Effects of various concentrations of Panobinostat on HMGB2 expression level in subcutaneous xenograft

high NAT10 expression in HCC exhibit significantly worse prognoses, substantiating NAT10's oncogenic properties. Silencing NAT10 significantly decreased ac4C levels and suppressed cell proliferation and invasion in HCC cells. Correspondingly, NAT10 silencing markedly inhibited liver tumor growth in a xenograft model and lung metastasis in mouse models. Therefore, NAT10/ac4C could serve as a potential predictive biomarker and therapeutic target for HCC.

Previous studies have demonstrated the role of ac4C in promoting the translation efficiency of multiple oncogene targets in Hela cells [11]. In HCC cells, we also confirm widespread mRNA acetylation within coding sequences, leading to enhanced global translation efficiency. Integrative acRIP-seq, RNA-seq, and Ribo-seq analysis identified HMGB2 as the top repressed gene in NAT10-knockdown cells. HMGB2 has been implicated in the progression of various cancers [51] and is notably upregulated in HCC, contributing to malignancy progression [39, 40]. Collectively, our study identifies a novel NAT10-ac4C-HMGB2 axis that plays a central role in NAT10's protumorigenic effect in HCC.

While it was previously believed that the N4-acetyl group of ac4C forms an intramolecular hydrogen bond, stabilizing a specific cytidine conformation that enhances Watson-Crick base pairing with guanosine [52–54], our study sheds light on the mechanism underlying ac4C's role in promoting translation elongation within the coding sequence region. Through mass spectrometry analysis using acetylated and non-acetylated versions of an oligo-RNA, we identified eEF2 and SRP68 as direct binders exclusively to ac4C-modified RNA. Furthermore, our results demonstrate that ac4C sites in the CDS of HMGB2 mRNA enhance eEF2 binding, thereby promoting translation elongation of HMGB2 mRNA. In this study, we have provided initial evidence of the function of eEF2, while SRP68 emerges as a promising recognition protein to elucidate the regulation of ac4C on mRNA translation in future investigations. Additionally, previous study have revealed that ac4C impacts mRNA stability [11], and the presence of 5′ UTR ac4C within Kozak sequences promotes upstream initiation while inhibiting canonical start codons [10]. We speculate that RNA binding proteins are involved in this process, and identifying the key proteins in future research could signify a significant advancement in the field of ac4C modification.

Regarding NAT10 inhibition, while Remodelin has shown promising preclinical efficacy in models of Hutchinson-Gilford Progeria Syndrome (HGPS) by inhibiting NAT10 lysine acetyltransferase (KAT) activity [11, 55], it does not inhibit NAT10-dependent cytidine acetylation [44], Our data also indicate that Remodelin does not effectively inhibit tumor cell ac4C modification or modulate the expression of HMGB2, raising doubts about its specificity as an RNA acetylation inhibitor for NAT10. However, we discovered Panobinostat through structure-based virtual screening, as a lead compound that directly binds to NAT10's catalytic pocket (G641) and effectively suppresses NAT10's ac4C acetyltransferase activity. Notably, Panobinostat exhibits promising anti-HCC efficacy both in vitro and in vivo with minimal side effects, positioning it as a potential NAT10/ac4C inhibitor for further clinical exploration.

The present study has some limitations. Firstly, we focused solely on the single gene regulation of NAT10/ac4C/HMGB2 and did not explore the signaling pathways involved in NAT10 or HMGB2. Additionally, the use of knockout (KO) mice or hydrodynamic mouse models could provide further insights into the relationship between NAT10/ac4C and the immune microenvironment. Moreover, further identification of the binding site of Panobinostat on NAT10 could lead to the development of drugs with better specificity.

5 | CONCLUSIONS

In the present study, we identified that aberrant upregulation of HMGB2 in HCC is triggered by NAT10-mediated ac4C modification. As a functional target of NAT10, it stimulates ac4C modification within the CDS of HMGB2 mRNA, thereby enhancing HMGB2 translation. Furthermore, we have unveiled eEF2 as a novel reader of ac4C-modified mRNA, demonstrating its binding to ac4C sites within HMGB2 mRNA's CDS and promoting HMGB2 translation. Notably, our investigation has pinpointed Panobinostat as a potent NAT10-ac4C inhibitor, effectively impeding HCC progression. In summary, our

model. (H) Representative IHC images of HMGB2 expression in subcutaneous xenograft model (scale bar: 20 μm). (I) Liver orthotopic implantation models transplanted with indicated cells (scale bar: 1000 μm). Representative bioluminescence imaging of mice (left panel) and quantification of tumor nodules (right panel) (0 mg, $n = 8$; 5-10 mg, $n = 10$). (J) Lung metastasis model transplanted with indicated cells (scale bar: 1000 μm). Representative bioluminescence imaging of mice (left panel) and quantification of lung metastatic nodules (right panel) ($n = 9$). (K) Graphic illustration depicts how NAT10 modulates ac4C-mediated translation elongation to promote HCC progression. (A-C) Data is shown as mean ± SD, $n = 3$. Statistical analysis: Unpaired t-tests. $^{**}P < 0.01$, $^{***}P < 0.001$. Abbreviations: IC50, a half-maximal inhibitory concentration; ac4C, N4-acetylcytidine; NAT10, N-acetyltransferase 10; HMGB2, High Mobility Group Protein B2; IHC, immunohistochemistry; SD, standard deviation.

studies illuminate the critical role of NAT10-mediated mRNA ac4C modification in HCC development and highlight the therapeutic potential of NAT10/ac4C as a target for HCC treatment.

AUTHOR CONTRIBUTIONS

Bixiang Zhang, Zeyang Ding, Jiefeng He, and Xiaoping Chen conceived, supervised, analyzed and interpreted the study, and provided a critical review. Hailing Liu carried out the experiments, statistical analysis, and manuscript preparation. Lei Xu, Shiwei Yue, Hongfei Su, and Xing Chen provided clinical specimens and made clinical pathology evaluations. Hailing Liu wrote the manuscript and Bixiang Zhang reviewed and edited the manuscript. Qiumeng Liu, Hui Li, and Huifang Liang offered technical support and relevant advice.

ACKNOWLEDGMENTS

We thank Chuan He (The University of Chicago, Chicago, USA) for helpful suggestions. We thank Yi Hu and Wuhan Metware Biotechnology Co.Ltd for their UPLC-MS/MS technique support. We are most grateful to Yan Wang and Yuan Sun (Institute of Hydrobiology, Chinese Academy of Sciences) for technical assistance in vivo imaging system. We also thank Prof. Yan Li (Zhongnan Hospital of Wuhan University, Wuhan, China) for kindly supplying HCCLM9 cells. This research was supported by the National Natural Science Foundation of China (grant 81874189 to Bixiang Zhang, grant 82273441 and 81874065 to Zeyang Ding and grant 82203823 to Hui Li), State Key Project on Infection Disease of China (grant 2018ZX10723204-003-003 to Xiaoping Chen), National Basic Research Program of China (grant 2020YFA0710700 to Zeyang Ding), the first level of the public health youth top talent project of Hubei province (grant No. 2022SCZ051 to Zeyang Ding), Knowledge Innovation Program of Wuhan-Shuguang Project (grant No. 2022020801020456 to Zeyang Ding), and Tongji Hospital (HUST) Foundation for Excellent Young Scientist (grant No. 2020YQ05 to Zeyang Ding).

CONFLICT OF INTEREST STATEMENT

All authors declare no competing interests.

DATA AVAILABILITY STATEMENT

The RNA sequencing (RNA-seq) data of the HCC cohorts in the Cancer Genome Atlas project (TCGA-LIHC) were collected from the UCSC Xena public data hub (http://xena.ucsc.edu/public/). Microarray or RNA-seq data of 89 HCC cohorts were analyzed using the online tool Integrative HCC Gene Analysis (IHGA) (https://www.hccdatasph.cn/app/ihga). Proteomic data of HCC patients were downloaded from the National Cancer Institute's Clinical Proteomic Tumor Analysis Consortium (CPTAC, https://proteomics.cancer.gov/programs/cptac). The data generated in this study are available upon request from the corresponding authors.

ETHICS APPROVAL AND CONSENT TO PARTICIPATE

This study was approved by the Clinical Research Ethics Committee of Tongji Hospital (HUST, Wuhan, China) (permit number: TJ-IRB20211163). Written informed consents were received from all patients. All animal studies were conducted in accordance with the Ethics Committee of Tongji Hospital (HUST, Wuhan, China) (permit number: TJH-202110006).

ORCID

Hailing Liu https://orcid.org/0000-0002-7022-0602
Shiwei Yue https://orcid.org/0009-0007-8284-4555
Hongfei Su https://orcid.org/0009-0003-4739-262X
Huifang Liang https://orcid.org/0000-0001-6874-3634
Bixiang Zhang https://orcid.org/0000-0002-1609-7260

REFERENCES

1. Devarbhavi H, Asrani SK, Arab JP, Nartey YA, Pose E, Kamath PS. Global burden of liver disease: 2023 update. J Hepatol. 2023;79(2):516-37.
2. El-Khoueiry AB, Sangro B, Yau T, Crocenzi TS, Kudo M, Hsu C, et al. Nivolumab in patients with advanced hepatocellular carcinoma (CheckMate 040): an open-label, non-comparative, phase 1/2 dose escalation and expansion trial. Lancet. 2017;389(10088):2492-502.
3. Llovet JM, Kelley RK, Villanueva A, Singal AG, Pikarsky E, Roayaie S, et al. Hepatocellular carcinoma. Nat Rev Dis Primers. 2021;7(1):6.
4. Finn RS, Qin S, Ikeda M, Galle PR, Ducreux M, Kim TY, et al. Atezolizumab plus Bevacizumab in Unresectable Hepatocellular Carcinoma. N Engl J Med. 2020;382(20):1894-905.
5. Llovet JMRS, Mazzaferro V, Hilgard P, Gane E, Blanc JF, de Oliveira AC, et al. Sorafenib in advanced hepatocellular carcinoma. N Engl J Med. 2008;359(4):378-90.
6. Rizzo ARA, Brandi G. Systemic adjuvant treatment in hepatocellular carcinoma: tempted to do something rather than nothing. Future Oncol. 2020;16(32):2587-2589.
7. Rizzo ARA, Brandi G. Immune-based combinations for advanced hepatocellular carcinoma: shaping the direction of first-line therapy. Future Oncol. 2021;17(7):755-757.
8. Bortolin-Cavaille ML, Quillien A, Thalalla Gamage S, Thomas JM, Sas-Chen A, Sharma S, et al. Probing small ribosomal subunit RNA helix 45 acetylation across eukaryotic evolution. Nucleic Acids Res. 2022;50(11):6284-99.
9. Sharma S, Langhendries JL, Watzinger P, Kotter P, Entian KD, Lafontaine DL. Yeast Kre33 and human NAT10 are conserved 18S rRNA cytosine acetyltransferases that modify tRNAs assisted by the adaptor Tan1/THUMPD1. Nucleic Acids Res. 2015;43(4):2242-58.
10. Arango D, Sturgill D, Yang R, Kanai T, Bauer P, Roy J, et al. Direct epitranscriptomic regulation of mammalian translation

initiation through N4-acetylcytidine. Mol Cell. 2022;82(15):2797-814 e11.
11. Arango D, Sturgill D, Alhusaini N, Dillman AA, Sweet TJ, Hanson G, et al. Acetylation of Cytidine in mRNA Promotes Translation Efficiency. Cell. 2018;175(7):1872-86 e24.
12. Wang K, Zhou LY, Liu F, Lin L, Ju J, Tian PC, et al. PIWI-Interacting RNA HAAPIR Regulates Cardiomyocyte Death After Myocardial Infarction by Promoting NAT10-Mediated ac(4) C Acetylation of Tfec mRNA. Adv Sci (Weinh). 2022;9(8):e2106058.
13. Yang W, Li HY, Wu YF, Mi RJ, Liu WZ, Shen X, et al. ac4C acetylation of RUNX2 catalyzed by NAT10 spurs osteogenesis of BMSCs and prevents ovariectomy-induced bone loss. Mol Ther Nucleic Acids. 2021;26:135-47.
14. Hao H, Liu W, Miao Y, Ma L, Yu B, Liu L, et al. N4-acetylcytidine regulates the replication and pathogenicity of enterovirus 71. Nucleic Acids Res. 2022;50(16):9339-54.
15. Tsai K, Jaguva Vasudevan AA, Martinez Campos C, Emery A, Swanstrom R, Cullen BR. Acetylation of Cytidine Residues Boosts HIV-1 Gene Expression by Increasing Viral RNA Stability. Cell Host Microbe. 2020;28(2):306-12 e6.
16. Jiang X, Cheng Y, Zhu Y, Xu C, Li Q, Xing X, et al. Maternal NAT10 orchestrates oocyte meiotic cell-cycle progression and maturation in mice. Nat Commun. 2023;14(1):3729.
17. Chen L, Wang WJ, Liu Q, Wu YK, Wu YW, Jiang Y, et al. NAT10-mediated N4-acetylcytidine modification is required for meiosis entry and progression in male germ cells. Nucleic Acids Res. 2022;50(19):10896-913.
18. Xie R, Cheng L, Huang M, Huang L, Chen Z, Zhang Q, et al. NAT10 Drives Cisplatin Chemoresistance by Enhancing ac4C-Associated DNA Repair in Bladder Cancer. Cancer Res. 2023;83(10):1666-1683.
19. Liao L, He Y, Li SJ, Yu XM, Liu ZC, Liang YY, et al. Lysine 2-hydroxyisobutyrylation of NAT10 promotes cancer metastasis in an ac4C-dependent manner. Cell Res. 2023;33(5):355-71.
20. Jin C, Wang T, Zhang D, Yang P, Zhang C, Peng W, et al. Acetyltransferase NAT10 regulates the Wnt/beta-catenin signaling pathway to promote colorectal cancer progression via ac(4)C acetylation of KIF23 mRNA. J Exp Clin Cancer Res. 2022;41(1):345.
21. Chen X, Hao Y, Liu Y, Zhong S, You Y, Ao K, et al. NAT10/ac4C/FOXP1 Promotes Malignant Progression and Facilitates Immunosuppression by Reprogramming Glycolytic Metabolism in Cervical Cancer. Adv Sci (Weinh). 2023;10(32):e2302705.
22. Rui Ma JC, Shaojie Jiang, Shuang Lin, Xiuming Zhang, Xiao Liang. Up regulation of NAT10 promotes metastasis of hepatocellular carcinoma cells through epithelial-to-mesenchymal transition. Am J Transl Res. 2016;8(10):4215-4223.
23. Pan Z, Bao Y, Hu M, Zhu Y, Tan C, Fan L, et al. Role of NAT10-mediated ac4C-modified HSP90AA1 RNA acetylation in ER stress-mediated metastasis and lenvatinib resistance in hepatocellular carcinoma. Cell Death Discov. 2023;9(1):56.
24. Tan Y, Zheng J, Liu X, Lu M, Zhang C, Xing B, Du X. Loss of nucleolar localization of NAT10 promotes cell migration and invasion in hepatocellular carcinoma. Biochem Biophys Res Commun. 2018;499(4):1032-8.
25. Li Q, Liu X, Jin K, Lu M, Zhang C, Du X. NAT10 is upregulated in hepatocellular carcinoma and enhances mutant p53 activity. BMC Cancer. 2017;17(1):605.
26. Roundtree IA, Evans ME, Pan T, He C. Dynamic RNA Modifications in Gene Expression Regulation. Cell. 2017;169(7):1187-200.
27. Liu H, Lan T, Li H, Xu L, Chen X, Liao H, et al. Circular RNA circDLC1 inhibits MMP1-mediated liver cancer progression via interaction with HuR. Theranostics. 2021;11(3):1396-411.
28. Weichert W, Roske A, Gekeler V, Beckers T, Ebert MP, Pross M, et al. Association of patterns of class I histone deacetylase expression with patient prognosis in gastric cancer: a retrospective analysis. Lancet Oncol. 2008;9(2):139-48.
29. Wang X, Zhao BS, Roundtree IA, Lu Z, Han D, Ma H, et al. N(6)-methyladenosine Modulates Messenger RNA Translation Efficiency. Cell. 2015;161(6):1388-99.
30. Love MI, Huber W, Anders S. Moderated estimation of fold change and dispersion for RNA-seq data with DESeq2. Genome Biol. 2014;15(12):550.
31. de Klerk E, Fokkema IF, Thiadens KA, Goeman JJ, Palmblad M, den Dunnen JT, et al. Assessing the translational landscape of myogenic differentiation by ribosome profiling. Nucleic Acids Res. 2015;43(9):4408-28.
32. Su R, Dong L, Li C, Nachtergaele S, Wunderlich M, Qing Y, et al. R-2HG Exhibits Anti-tumor Activity by Targeting FTO/m(6)A/MYC/CEBPA Signaling. Cell. 2018;172(1-2):90-105 e23.
33. Martinez Molina D, Jafari R, Ignatushchenko M, Seki T, Larsson EA, Dan C, et al. Monitoring drug target engagement in cells and tissues using the cellular thermal shift assay. Science. 2013;341(6141):84-7.
34. Schmidt EK, Clavarino G, Ceppi M, Pierre P. SUnSET, a nonradioactive method to monitor protein synthesis. Nat Methods. 2009;6(4):275-7.
35. Halgren TA. Merck Molecular Force Field. I. Basis, Form, Scope, Parameterization, and Performance of MMFF94*. J Comput Chem. 1996;17(Nos. 5&6):490-519.
36. Jumper J, Evans R, Pritzel A, Green T, Figurnov M, Ronneberger O, et al. Highly accurate protein structure prediction with AlphaFold. Nature. 2021;596(7873):583-9.
37. Morris GM, Huey R, Lindstrom W, Sanner MF, Belew RK, Goodsell DS. AutoDock4 and AutoDockTools4: Automated docking with selective receptor flexibility. J Comput Chem. 2009;30(16):2785-91.
38. Cancer Genome Atlas Research Network. Electronic address wbe, Cancer Genome Atlas Research N. Comprehensive and Integrative Genomic Characterization of Hepatocellular Carcinoma. Cell. 2017;169(7):1327-41 e23.
39. Kwon JH, Kim J, Park JY, Hong SM, Park CW, Hong SJ, et al. Overexpression of high-mobility group box 2 is associated with tumor aggressiveness and prognosis of hepatocellular carcinoma. Clin Cancer Res. 2010;16(22):5511-21.
40. Pu J, Tan C, Shao Z, Wu X, Zhang Y, Xu Z, et al. Long Noncoding RNA PART1 Promotes Hepatocellular Carcinoma Progression via Targeting miR-590-3p/HMGB2 Axis. Onco Targets Ther. 2020;13:9203-11.
41. Dominissini D, Moshitch-Moshkovitz S, Schwartz S, Salmon-Divon M, Ungar L, Osenberg S, et al. Topology of the human and mouse m6A RNA methylomes revealed by m6A-seq. Nature. 2012;485(7397):201-6.

42. Huang H, Weng H, Sun W, Qin X, Shi H, Wu H, et al. Recognition of RNA N(6)-methyladenosine by IGF2BP proteins enhances mRNA stability and translation. Nat Cell Biol. 2018;20(3): 285-95.
43. Xiang Y, Zhou C, Zeng Y, Guo Q, Huang J, Wu T, et al. NAT10-Mediated N4-Acetylcytidine of RNA Contributes to Post-transcriptional Regulation of Mouse Oocyte Maturation in vitro. Front Cell Dev Biol. 2021;9:704341.
44. Shrimp JH, Jing Y, Gamage ST, Nelson KM, Han J, Bryson KM, et al. Remodelin Is a Cryptic Assay Interference Chemotype That Does Not Inhibit NAT10-Dependent Cytidine Acetylation. ACS Med Chem Lett. 2021;12(6):887-92.
45. Deng M, Zhang L, Zheng W, Chen J, Du N, Li M, et al. Helicobacter pylori-induced NAT10 stabilizes MDM2 mRNA via RNA acetylation to facilitate gastric cancer progression. J Exp Clin Cancer Res. 2023;42(1):9.
46. Xie L, Zhong X, Cao W, Liu J, Zu X, Chen L. Mechanisms of NAT10 as ac4C writer in diseases. Mol Ther Nucleic Acids. 2023;32:359-68.
47. Luo J, Cao J, Chen C, Xie H. Emerging role of RNA acetylation modification ac4C in diseases: Current advances and future challenges. Biochem Pharmacol. 2023;213:115628.
48. Wang G, Zhang M, Zhang Y, Xie Y, Zou J, Zhong J, et al. NAT10-mediated mRNA N4-acetylcytidine modification promotes bladder cancer progression. Clinical and Translational Medicine. 2022;12(5):e738.
49. Yang Q, Lei X, He J, Peng Y, Zhang Y, Ling R, et al. N4-Acetylcytidine Drives Glycolysis Addiction in Gastric Cancer via NAT10/SEPT9/HIF-1alpha Positive Feedback Loop. Adv Sci (Weinh). 10(23):e2300898.
50. Zheng X, Wang Q, Zhou Y, Zhang D, Geng Y, Hu W, et al. N-acetyltransferase 10 promotes colon cancer progression by inhibiting ferroptosis through N4-acetylation and stabilization of ferroptosis suppressor protein 1 (FSP1) mRNA. Cancer Commun (Lond). 2022;42(12):1347-66.
51. Starkova T, Polyanichko A, Tomilin AN, Chikhirzhina E. Structure and Functions of HMGB2 Protein. Int J Mol Sci. 2023; 24(9):8334.
52. Kumbhar BV, Kamble AD, Sonawane KD. Conformational preferences of modified nucleoside N(4)-acetylcytidine, ac4C occur at "wobble" 34th position in the anticodon loop of tRNA. Cell Biochem Biophys. 2013;66(3):797-816.
53. Parthasarathy R GS, De NC, Chheda GB. Conformation of N4-acetylcytidine, a modified nucleoside of tRNA, and stereochemistry of codon-anticodon interaction. Biochem Biophys Res Commun. 1978 83(2):657-63.
54. Stern L SL. The role of the minor base N4-acetylcytidine in the function of the Escherichia coli noninitiator methionine transfer RNA. J Biol Chem. 1978;253(17):6132-9.
55. Ito S, Horikawa S, Suzuki T, Kawauchi H, Tanaka Y, Suzuki T. Human NAT10 is an ATP-dependent RNA acetyltransferase responsible for N4-acetylcytidine formation in 18 S ribosomal RNA (rRNA). J Biol Chem. 2014;289(52):35724-30.

SUPPORTING INFORMATION

Additional supporting information can be found online in the Supporting Information section at the end of this article.

How to cite this article: Liu H, Xu L, Yue S, Su H, Chen X, Liu Q, et al. Targeting N4-acetylcytidine suppresses hepatocellular carcinoma progression by repressing eEF2-mediated HMGB2 mRNA translation. Cancer Commun. 2024;44:1018–1041. https://doi.org/10.1002/cac2.12595